Cell autonomous role of leucine-rich repeat kinase in protection of dopaminergic neuron survival

Jongkyun Kang[1¶], Guodong Huang[1¶], Long Ma[1], Youren Tong[1], Phoenix Chen[1], and Jie Shen[1,2*]

[1]Department of Neurology, Brigham and Women's Hospital, [2]Program in Neuroscience, Harvard Medical School, Boston, MA 02445, United States of America

*Corresponding author

E-mail: jshen@bwh.harvard.edu

[¶]These authors contributed equally to this work.

Abstract

Mutations in leucine-rich repeat kinase 2 (LRRK2) are the most common genetic cause of Parkinson's disease (PD), which is the leading neurodegenerative movement disorder characterized by the progressive loss of dopaminergic (DA) neurons in the substantia nigra pars compacta (SNpc). However, whether LRRK2 mutations cause PD and degeneration of DA neurons *via* a toxic gain-of-function or a loss-of-function mechanism is unresolved and has pivotal implications in LRRK2 based PD therapy. In this study, we investigate whether LRRK2 and its functional homologue LRRK1 play an essential, intrinsic role in DA neuron survival through the development of DA neuron-specific *LRRK* conditional double knockout (cDKO) mice. We first generated and characterized floxed *LRRK1* and *LRRK2* mice and then confirmed that germline deletions of the floxed *LRRK1* and *LRRK2* alleles result in null alleles, as evidenced by the absence of *LRRK1* and *LRRK2* mRNA and protein in the respective homozygous deleted mutant mice. We further examined the specificity of Cre-mediated recombination driven by the *dopamine transporter-Cre* (*DAT-Cre*) knockin (KI) allele using a GFP reporter line and confirmed that *DAT-Cre*-mediated recombination is restricted to DA neurons in the SNpc. Crossing these validated floxed *LRRK1* and *LRRK2* mice with *DAT-Cre* KI mice, we then generated DA neuron-restricted *LRRK* cDKO mice and further showed reduced levels of LRRK1 and LRRK2 in dissected ventral midbrains of *LRRK* cDKO mice. While DA neuron-restricted *LRRK* cDKO mice of both sexes exhibit normal mortality and body weight, they develop age-dependent loss of DA neurons in the SNpc, as demonstrated by the progressive reduction of DA neurons in the SNpc of cDKO mice at 20 and 24 months of age. Moreover, DA neurodegeneration is accompanied with increases of apoptosis and elevated microgliosis in the SNpc of *LRRK* cDKO mice. These findings provide unequivocal evidence for the importance of LRRK in DA neurons and raise the possibility that LRRK2 mutations may impair its protection of DA neurons, leading to the loss of DA neurons in Parkinson's disease.

Introduction

Parkinson's disease (PD) is the most common movement disorder and is characterized by the progressive loss of dopaminergic (DA) neurons in the substantia nigra pars compacta (SNpc). Dominantly inherited missense mutations in the *leucine-rich repeat kinase 2* (*LRRK2*) gene are the most common cause of both familial and sporadic PD, highlighting the importance of LRRK2 in PD pathogenesis (1-16). LRRK2 is a large protein of 2,527 amino acid residues containing several functional domains including several leucine-rich repeats (LRRs), a GTPase-like domain of Ras-of-complex (Roc), a C-terminal of Roc (COR) domain, and a serine/threonine MAPKKK-like kinase domain. LRRK1, a homologue of LRRK2, belongs to the evolutionarily conserved Roco protein family and contains similar LRRs, Roc, COR, and kinase domains (17-19). LRRK proteins are broadly expressed with LRRK2 being most abundant in the kidney (20). While most PD mutations are found in LRRK2, rare variants in the Roc, COR, and kinase domains of LRRK1 have been reported and may be associated with PD (21). Furthermore, the Roc-COR domain of LRRK2 forms dimers and exhibits conventional Ras-like GTPase properties, and the R1441/C/G/H and I1371V mutations destabilize dimer formation and decrease GTPase activity (22, 23). Recent high-resolution cryoEM structural studies of full-length LRRK2 demonstrated its existence as dimers and pathogenic mutations such as R1441/C/G/H and Y1699I at the Roc-COR interface, whereas the G2910S mutant and wild-type LRRK2 share similar structure (24).

Previous genetic studies demonstrated that LRRK2 plays essential roles in the autophagy-lysosomal pathway (25-28). Consistent with abundant expression of LRRK2 in kidneys, *LRRK2*-/- mice develop age-dependent phenotypes in the kidney, including autophagy-lysosomal impairments and increases of α-synuclein, apoptosis, and inflammatory responses (25, 26, 29). It has also been reported that LRRK2 is important for maintaining lung homeostasis, and *LRRK2* deficiency results in impaired autophagy in alveolar type II epithelial cells (28). It was proposed that the lack of brain phenotypes in *LRRK2*-/- mice might be due to the presence of LRRK1 and potential functional compensation mechanisms (25, 26). Indeed, *LRRK* double knockout (DKO) mice develop age-dependent, progressive loss of DA neurons in the SNpc, beginning at 14 months of age (30). However, *LRRK* DKO mice also

73 exhibit lower body weight and increased mortality, raising the possibility that DA neurodegeneration in
74 *LRRK* DKO mice may be secondary to poor health.

75 In this study, we investigate whether LRRK2 and its functional homologue LRRK1 play an
76 essential, intrinsic role in DA neuron survival through the development of DA neuron-specific *LRRK*
77 conditional DKO (cDKO) mice. We first generated and confirmed floxed *LRRK1* and *LRRK2* mice, and
78 then crossed them with the deleter *CMV-Cre* to create germline deletions of the floxed *LRRK1* and
79 *LRRK2* alleles, followed by Northern and Western analyses to confirm the absence of *LRRK1* and *LRRK2*
80 mRNA and protein in the respective homozygous deleted mutant mice. We also crossed a GFP reporter
81 mouse with *DAT-Cre* KI mice and found that Cre-mediated recombination occurs in most, if not all, DA
82 neurons and is restricted to DA neurons in the SNpc. We then crossed these thoroughly validated floxed
83 *LRRK1* and *LRRK2* mice with *DAT-Cre* KI mice to generate DA neuron-restricted *LRRK* cDKO mice and
84 further confirmed the reduction of LRRK1 and LRRK2 in dissected ventral midbrains of *LRRK* cDKO
85 mice. While DA neuron-restricted *LRRK* cDKO mice of both sexes exhibit normal mortality and body
86 weight, they develop age-dependent loss of DA neurons in the SNpc, as demonstrated by the progressive
87 reduction of TH+ DA neurons or NeuN+ neurons in the SNpc of cDKO mice at 20 and 24 months of age.
88 Interestingly, quantitative electron microscopy analysis showed a similar number of electron-dense
89 vacuoles in SNpc neurons of *LRRK* cDKO mice relative to controls, in contrast to age-dependent,
90 dramatic increases of vacuoles in SNpc neurons of germline *LRRK* DKO mice (30, 31). Moreover, DA
91 neurodegeneration is accompanied with increases of apoptosis and elevated microgliosis in the SNpc of
92 *LRRK* cDKO mice. These findings provide unequivocal evidence for the importance of LRRK in DA
93 neurons and raise the possibility that LRRK2 mutations may impair this crucial physiological function,
94 leading to the loss of DA neurons in Parkinson's disease.

95 **Results**

96 **Generation and molecular characterization of the floxed and deleted *LRRK1* and *LRRK2* alleles**

97 LRRK2 and its homologue LRRK1 share several functional (LRRs, GTPase Roc, COR, and
98 kinase) domains (Figure 1A). To investigate the intrinsic role of LRRK in DA neurons, we generated
99 floxed *LRRK1* (*fLRRK1*) and floxed *LRRK2* (*fLRRK2*) mice, which permit deletions of *LRRK1* and
100 *LRRK2* selectively in DA neurons by *DAT-Cre*, which expresses Cre recombinase under the control of the
101 endogenous *DAT* promoter (32). We introduced two *loxP* sites in introns 26 and 29 of *LRRK1* through
102 homologous recombination and site-specific recombination by FLP recombinase to remove the positive
103 selection *PGK-neo* cassette, which is flanked by two *FRT* sites (Figure 1B, C; Figure 1-figure supplement
104 1, 2). The embryonic stem (ES) cells carrying the targeted allele or the floxed allele were identified and
105 validated by Southern analysis using the 5' and 3' external probes as well as the *neo* probe (Figure 1D;
106 Figure 1-figure supplement 3). The validated ES cells carrying the floxed *LRRK1* allele were injected into
107 mouse blastocysts to develop floxed *LRRK1* mice, which were further confirmed by Southern using the 5'
108 and 3' external probes (Figure 1D). In the presence of Cre recombinase, the floxed *LRRK1* region
109 containing part of intron 26 (1,288 bp), exons 27-29, which encode the kinase domain, and part of intron
110 29 (1,023 bp) is deleted (Figure 1C), and the removal of exons 27-29 (625 bp) results in a frameshift of
111 downstream codons.

112 The *LRRK2* targeting vector contains the 5' homologous region, a *loxP* site 1,768 bp upstream of
113 the transcription initiation site, exons 1-2, the *PGK-neo* cassette flanked by two *loxP* sites and two *FRT*
114 sequences, and the 3' homologous region (Figure 1B, E; Figure 1-figure supplement 4, 5). The ES cell
115 clones carrying the targeted allele were identified and validated by Southern analysis using the 5' external
116 probe (Figure 1F; Figure 1-figure supplement 6) and genomic PCR followed by sequencing. Mice
117 carrying the *LRRK2* targeted allele were further verified by Southern analysis using the 5' and 3' external
118 probes (Figure 1-figure supplement 6) as well as the *neo* probe and were then crossed with the *Actin-FLP*
119 mice (33) to remove the *PGK-neo* cassette flanked by two *FRT* sites to generate floxed *LRRK2* mice
120 (Figure 1E). The resulting floxed *LRRK2* mice were confirmed by Southern analysis using the 5' and 3'
121 external probes (Figure 1F). In the presence of Cre recombinase, the floxed *LRRK2* region containing the
122 promoter and exons 1-2 are deleted, likely resulting in a null allele, as we previously targeted a very

123 similar region (~2.5 kb upstream of the transcription initiation site and exons 1-2) to generate germline
124 deletion of *LRRK2* (25).

125 Dopaminergic neurons in the SNpc are a small neuronal population embedded in the ventral
126 midbrain, making it difficult to confirm whether DA neuron-specific deletions of the floxed *LRRK1* and
127 *LRRK2* regions result in null alleles. We previously generated three independent *LRRK1* knockout (KO)
128 mice, and only one KO line (Line 2) represents a *LRRK1* null allele (30), whereas deletion of *LRRK2*
129 promoter region and exons 1-2 resulted in a *LRRK2* null allele (25). We therefore generated germline
130 deleted *LRRK1* and *LRRK2* mice from floxed *LRRK1* and *LRRK2* mice, respectively, by crossing them to
131 germline deleter *CMV-Cre* transgenic mice (34).

132 We then performed Northern analysis of *LRRK1* using both an upstream probe specific for exons
133 2-3 and a downstream probe specific for exons 27-29 (Figure 1G; Figure 1-figure supplement 7, 8).
134 Because of the low expression level of *LRRK1* and the relative abundance of *LRRK1* in the lung (20), we
135 enriched polyA+ RNA from the lung of the mice carrying homozygous germline deleted (Δ/Δ) *LRRK1*
136 alleles derived from the floxed *LRRK1* alleles. Using a probe specific for exons 2-3, the *LRRK1*
137 transcripts in wild-type mice are the expected size of ~7.4 kb, whereas the detected *LRRK1* transcripts in
138 *LRRK1* Δ/Δ mice are smaller, consistent with the deletion of exons 27-29 (625 bp), resulting in a
139 frameshift of downstream codons and the likely degradation of the truncated *LRRK1* mRNA (Figure. 1G;
140 Figure 1-figure supplement 8). Using a probe specific for exons 27-29, there is no *LRRK1* transcript in
141 *LRRK1* Δ/Δ mice (Figure. 1G; Figure 1-figure supplement 8). Extensive RT-PCR analysis of total RNA
142 isolated from the kidney, brain, and lung of *LRRK1* Δ/Δ mice using an exon 32-specific primer for RT
143 and exon-specific primer sets for PCR (*e.g.* exons 4-8, 11-17, 20-25, and 25-31), followed by sequencing
144 confirmation of the PCR products, indicated normal *LRRK1* splicing in *fLRRK1/fLRRK1* mice and the
145 lack of *LRRK1* exons 27-29 in *LRRK1* Δ/Δ mice (Figure 1-figure supplement 9).

146 Similarly, Northern analysis of *LRRK2* using a probe specific for exons 1-5 and RT-PCR
147 followed by sequencing confirmed the absence of *LRRK2* mRNA in *LRRK2* Δ/Δ brains and normal

148 *LRRK2* transcripts in *fLRRK2/fLRRK2* brains (Figure 1H; Figure 1-figure supplement 10, 11).
149 Furthermore, Western analysis confirmed the absence of LRRK1 and LRRK2 proteins in the brain of
150 *LRRK1* Δ/Δ and *LRRK2* Δ/Δ mice, respectively (Fig. 1I). Taken together, our Northern, RT-PCR followed
151 by sequencing, and Western analyses demonstrated that deletion of the floxed *LRRK1* and *LRRK2* alleles
152 results in null mutations. Thus, floxed *LRRK1* and *LRRK2* alleles can be used to generate DA neuron-
153 specific *LRRK* cDKO mice.

154 **Generation and molecular characterization of DA neuron-specific *LRRK* cDKO mice**

155 To generate DA neuron-specific *LRRK* cDKO mice, we used *DAT-Cre* KI mice, which express
156 Cre recombinase under the control of the endogenous *DAT* promoter (32). To confirm if Cre-mediated
157 recombination occurs broadly and specifically in DA neurons of the SNpc, we crossed *DAT-Cre* mice
158 with the *Rosa26-CAG-LSL-ZsGreen1* reporter mouse (35). Upon Cre expression, Cre recombinase
159 removes the floxed "stop" cassette, resulting in the expression of EGFP. We found that Cre-mediated
160 recombination (GFP+) occurs in TH+ cells in the SNpc (Figure 2A). Quantification of GFP+ and/or TH+
161 cells in the SNpc showed that 99% of TH+ dopaminergic neurons are also GFP+, demonstrating that Cre-
162 mediated recombination takes place in essentially all DA neurons in the SNpc (Figure 2B).

163 Having confirmed *fLRRK1* and *fLRRK2* mice as well as *DAT-Cre* mice, we then bred them
164 together to generate *LRRK* cDKO mice (*fLRRK1/fLRRK1; fLRRK2/fLRRK2; DAT-Cre/+*), which were
165 further bred with *fLRRK1/fLRRK1; fLRRK2/fLRRK2* mice to generate cDKO and littermate controls
166 (*fLRRK1/fLRRK1; fLRRK2/fLRRK2*). It was previously reported that germline *LRRK* DKO mice failed to
167 gain weight as they aged (30). However, DA neuron-specific *LRRK* cDKO and littermate control mice
168 have similar body and brain weights at the ages of 2-24 months (Figure 2C, D). Western analysis showed
169 a significant reduction of LRRK1 and LRRK2 proteins in the dissected ventral midbrain but not in the
170 cerebral cortex of DA neuron-specific *LRRK* cDKO, relative to littermate controls at 2-3 months of age
171 (Figure 2E, F).

172 **Age-dependent loss of DA neurons in the SNpc of *LRRK* cDKO mice**

173 To determine whether the inactivation of LRRK selectively in DA neurons of the SNpc impacts
174 their survival, we performed TH immunostaining and quantified TH+ DA neurons in the SNpc of *LRRK*
175 cDKO mice and littermate controls. The morphology of TH+ DA neurons in *LRRK* cDKO mice at the
176 ages of 15, 20, and 24 months appears normal (Figure 3A). TH+ neuron counting revealed that the
177 number of DA neurons in the SNpc at the age of 15 months is similar between cDKO mice (10,000 ± 141)
178 and littermate controls (10,077 ± 310, $F_{1,46} = 16.59$, $p = 0.0002$; $p > 0.9999$, two-way ANOVA with
179 Bonferroni's post hoc multiple comparisons; Figure 3B). However, at the age of 20 months, the number
180 of TH+ neurons in the SNpc of cDKO mice (8,948 ± 273) is significantly reduced, compared to controls
181 (10,244 ± 220; $p = 0.0041$), and is further decreased at the age of 24 months (Control: 9,675 ± 232, cDKO:
182 8,188 ± 452; $p = 0.0010$).

183 We further performed TH and NeuN double immunostaining of *LRRK* cDKO and control mice at
184 24 months of age (Figure 3C), and found that the number of NeuN+ neurons is also significantly reduced
185 in the SNpc of cDKO mice (17,923 ± 813), compared to controls (21,907 ± 469, $p = 0.0006$, Student's *t*-
186 test; Figure 3D). The number of TH+/NeuN+ cells in the SNpc of *LRRK* cDKO mice (10,500 ± 644) is
187 also lower, compared to control mice (14,102 ± 310, $p = 0.0001$; Figure 3D). These data indicate that the
188 decreases in the number of TH+ cells are not due to decreases in TH expression in DA neurons, but rather
189 a result of the loss of DA neuron cell bodies in the SNpc of *LRRK* cDKO mice.

190 We further evaluated apoptosis in the SNpc of *LRRK* cDKO and littermate controls at the age of
191 24 months using an antibody specific for active Caspase-3 to label apoptotic cells. We observed increases
192 in apoptotic DA neurons, labeled by active Caspase-3+ and TH+ immunoreactivity, in the SNpc of *LRRK*
193 cDKO mice (Figure 4A). Quantification of active Caspase-3+/TH+ apoptotic DA neurons shows a
194 significant increase in the SNpc of *LRRK* cDKO mice (323 ± 38), compared to controls (157 ± 8, $p =$
195 0.0004, Student's *t*-test; Figure 4B). These results further support that LRRK plays an intrinsic role in the
196 survival of DA neurons in the SNpc during aging.

197 Previously, we reported the reduction of noradrenergic neurons in the locus coeruleus (LC) of
198 *LRRK* DKO mice (30). We therefore quantified TH+ noradrenergic neurons in the LC of *LRRK* cDKO

199 mice at the age of 24 months, and found a similar number of TH+ cells in the LC of *LRRK* cDKO and
200 littermate controls (Control: 3,419 ± 86, cDKO: 3,350 ± 99, p = 0.6057, Student's *t*-test; Figure 5A, B).
201 Further examination of the GFP reporter line crossed with *DAT-Cre* showed the lack of Cre-mediated
202 recombination in the LC (Figure 5C).

203 **Quantitative EM analysis of the SNpc in *LRRK* cDKO mice**

204 We previously reported striking age-dependent increases of electron-dense autophagic and
205 autolysosomal vacuoles as well as the presence of large lipofuscin granules in the surviving SNpc neurons
206 of *LRRK* DKO mice beginning at 10 months of age (30, 31). To determine whether selective inactivation
207 of LRRK in DA neurons similarly results in the accumulation of electron-dense autophagic and
208 autolysosomal vacuoles in the SNpc, we performed EM analysis in the SNpc of *LRRK* cDKO mice and
209 littermate controls at the ages of 25 months (Figure 6). We observed various electron-dense double
210 membrane autophagosomes and single membrane autolysosomes as well as lipofuscin granules composed
211 of lipid-containing residues of lysosomal digestion in the SNpc of *LRRK* cDKO and littermate control
212 mice (Figure 6C-F). Interestingly, there are similar numbers of electron-dense vacuoles in the SNpc of
213 *LRRK* cDKO mice and littermate controls at the age of 25 months (Control: 6.72 ± 0.43, cDKO: 6.99 ±
214 0.52, p = 0.6839, Student's *t*-test; Figure 6G). We also found no significant difference in the area of
215 electron-dense vacuoles in the SNpc between *LRRK* cDKO and littermate controls at the age of 25 months
216 (Control: 4.43 ± 0.44 μm^2; cDKO: 4.60 ± 0.49 μm^2, p = 0.8048; Figure 6G). The difference in age-
217 dependent accumulation of electron-dense vacuoles in the SNpc between germline DKO mice and DA
218 neuron-restricted cDKO suggests that LRRK in non-DA neurons such as microglia, which is lacking in
219 germline DKO but is expressed normally in cDKO mice, may play a more prominent role.

220 **Enhanced microgliosis in the SNpc of *LRRK* cDKO mice**

221 We further evaluated whether elevated microgliosis accompanies DA neurodegeneration in the
222 SNpc of *LRRK* cDKO mice. We performed immunohistochemical analysis of Iba1, which labels
223 microglia, and TH, which marks DA neurons and processes, thus showing the boundary of the SNpc

224 (Figure 7A-C). We found that the number of Iba1+ immunoreactive microglia is significantly increased in
225 the SNpc of *LRRK* cDKO mice at 15 months of age (2541.3 ± 193.0), compared to controls (1736.7 ±
226 82.9; $p = 0.0017$, two-way ANOVA with Bonferroni's post hoc multiple comparisons; Figure 7A, D).
227 The number of Iba1+ immunoreactive microglia in the SNpc of *LRRK* cDKO is further increased
228 compared to controls at the age of 20 (Control: 2426.0 ± 67.7, cDKO: 3639.0 ± 127.1, $p < 0.0001$; Figure
229 7B, D) and 25 months (Control: 2640.0 ± 187.1, cDKO: 4088.8 ± 100.3, $p < 0.0001$; Figure 7C, D).
230 These results show that despite the selective inactivation of LRRK in DA neurons of *LRRK* cDKO mice,
231 microgliosis accompanies DA neuronal loss in the SNpc.

232 **Discussion**

233 LRRK2 mutations represent ~5% familial and 1-2% of sporadic PD cases, and the G2019S
234 mutation is the most common mutation but with a higher age of onset and incomplete penetrance (74% at
235 age 79) (36). Despite the importance of LRRK2 in PD pathogenesis, whether LRRK2 mutations cause PD
236 *via* a loss-of-function or a gain-of-function mechanism remains highly debated and unresolved. Neither
237 *LRRK2*-deficient mice nor *LRRK2* R1441C and G2019S KI mice develop dopaminergic
238 neurodegeneration (25, 37, 38). It was proposed that the lack of brain phenotypes in *LRRK2*-/- mice might
239 be due to the presence of LRRK1 (25, 26), which is broadly expressed in the brain including the midbrain
240 (https://www.proteinatlas.org/ENSG00000154237-LRRK1/brain). Indeed, germline deletions of LRRK2
241 and LRRK1 result in age-dependent loss of DA neurons and increases of apoptosis and microgliosis in the
242 SNpc of *LRRK* DKO mice (30, 31). However, the pleiotropic roles of LRRK1 and LRRK2 in the kidney
243 (25, 26, 29), lung (28), and bone (39, 40), and the observed earlier mortality and lower body weight in
244 *LRRK* DKO mice raised the possibility that DA neurodegeneration in *LRRK* DKO mice may be due to
245 poor health.

246 In this study, we address this important question through the development of floxed *LRRK1* and
247 *LRRK2* mice (**Figure 1; Figure 1-figure supplement 1-11**), which permit the dissection of cell intrinsic
248 function of LRRK in DA neurons. We generated DA neuron-specific *LRRK* cDKO mice using the *DAT*-

249 *Cre* KI allele (32) to delete floxed *LRRK1* and *LRRK2* regions selectively in DA neurons. Indeed, using
250 an EGFP reporter line, we found that *DAT-Cre* drives Cre-mediated recombination in almost all DA
251 neurons in the SNpc (**Figure 2**). Unlike the *LRRK* germline DKO mice (30), DA neuron-specific *LRRK*
252 cDKO mice exhibit normal body weight and mortality during mouse lifespan (**Figure 2**). Importantly,
253 *LRRK* cDKO mice develop age-dependent DA neurodegeneration, as evidenced by progressive reductions
254 of DA neurons in the SNpc at the age of 20-24 months (**Figure 3**) and increases of apoptotic DA neurons
255 (**Figure 4**), whereas the number of noradrenergic neurons in the LC is uncaged, consistent with the lack
256 of Cre-mediated recombination in the LC by *DAT-Cre* (**Figure 5**). Interestingly, quantitative EM analysis
257 showed similar numbers of electron-dense vacuoles in the SNpc of *LRRK* cDKO and control mice even at
258 25 months of age (**Figure 6**), in contrast to dramatic, age-dependent increases of vacuoles in the SNpc of
259 *LRRK* DKO mice (30, 31). Lastly, DA neurodegeneration in the SNpc of *LRRK* cDKO mice is
260 accompanied with elevated microgliosis (**Figure 7**).

261 The toxic gain-of-function pathogenic mechanism was supported by earlier biochemical reports
262 showing that LRRK2 mutations (*e.g.* R1441C/G, G2019S) enhance kinase activity, leading to elevated
263 levels of pSer1292-LRRK2 (41), pSer935- LRRK2 (42, 43), pT73-Rab10, and pS106-Rab12 (44).
264 However, most transgenic mice overexpressing mutant LRRK2 did not produce neurodegeneration or DA
265 neuron loss (45-53), suggesting that enhanced kinase activity does not correlate with compromised DA
266 neuronal survival, though two reports showed that overexpression of LRRK2 G2019S but not R1441C
267 resulted in DA neurodegeneration (54, 55). Thus, further studies are needed to elucidate the differences of
268 these seemingly conflicting transgenic findings and to understand the differences between the R1441C
269 and G2019S mutations.

270 The loss-of-function pathogenic mechanism was supported by mouse knockout findings showing
271 that germline inactivation of LRRK results in age-dependent loss of DA neurons in the SNpc and DA
272 terminals in the striatum (30, 31). The current study demonstrated a cell intrinsic role of LRRK in support
273 of DA neuron survival in the SNpc of the aging brain, providing further genetic evidence of an essential,
274 cell autonomous requirement of LRRK in DA neuron survival. However, highly penetrant PD-linked

275 mutations are dominantly-inherited missense mutations (6) in LRRK2, and there have been no reported
276 deletion mutations that are linked to or causal of familial PD, despite various variants were reported in
277 LRRK2 and LRRK1 that are associated with sporadic PD (but not linked to familial PD). One plausible
278 explanation is that LRRK2 mutant may act in a dominant negative manner, inhibiting the activity of the
279 wild-type LRRK2. This notion is supported by structural studies showing that the GTPase domain forms
280 a dimer, and that the R1441/C/G/H and I1371V mutations destabilize dimer formation and decrease
281 GTPase activity (22). LRRK2 may function as a dimer, which is further supported by the crystal structure
282 of LRRK2's WD40 domain dimer at 2.6 Å resolution (56). Additional studies also suggested that LRRK2
283 functions as a dimer (57-59), and that LRRK2 and LRRK1 can form a heterodimer (60). Furthermore,
284 LRRK2 G2385R variant, a risk factor for PD (61-64), has been reported as a partial loss-of-function
285 mutation (65, 66). Future studies are needed to differentiate the possibility between a toxic gain-of-
286 function pathogenic mechanism vs. loss-of-function mutations exerting a dominant negative effect further
287 impairing LRRK2 activity of the wild-type protein encoded by the LRRK2 wild-type allele, as the gain-
288 of-function or loss-of-function pathogenic mechanism underlying LRRK2 mutations pivots opposing
289 LRRK2 based therapeutic development of PD therapies.

290 Finally, it was surprising to find no accumulation of autophagic and autolysosomal vacuoles in
291 SNpc neurons of *LRRK* cDKO mice, even at the age of 25 months. This suggests that non-dopaminergic
292 cells (*e.g.* microglia), in which LRRK expression is unaffected in cDKO mice but is absent in germline
293 DKO mice, may contribute to the dramatic phenotypic differences. Development of cell type-specific
294 cDKO mice, such as microglia-specific *LRRK* cDKO mice, would permit further dissection of cell
295 autonomous and non-cell autonomous role of LRRK in dopaminergic neuronal survival and whether glial
296 LRRK plays a more important role in the regulation of the autophagy-lysosomal pathway.
297

298 ## Materials and methods

299 **Key Resource Table**

Antibodies				
Reagent Name	**Source**	**Catalog #**	**Identifiers**	**Titer**
Rabbit anti-LRRK1	Alomone Lab	ANR-101	AB_2756700	WB: 1:1000
Rabbit anti-LRRK2	abcam	Ab133474	AB_2713963	WB: 1:1000
Mouse anti-α-Vinculin	Millipore	05-386	AB_309711	WB: 1:2000
Rabbit anti-GFP	abcam	ab290	AB_303395	IF: 1:1000
Mouse anti-TH	SantaCruz	Sc-25269	AB_628422	IF: 1:50
Rabbit anti-TH	abcam	Ab112	AB_297840	IHC: 1:750
Rabbit anti-NeuN	Cell Signaling Technology	12943S	AB_2630395	IF: 1:400
Rabbit anti-cleaved caspase-3	Cell Signaling Technology	9661	AB_2341188	IF: 1:150
Rabbit anti-Iba1	Wako	019-19741	AB_839504	IF: 1:500
Goat anti-rabbit IRdye800	LI-COR Biosciences	926-32211	AB_2651127	WB: 1:20000
Goat anti-mouse IRdye680	LI-COR Biosciences	926-68020	AB_2651128	WB: 1:20000
Alexa Fluor 488 goat anti-mouse IgG	ThermoFisher Scientific	A-11001	AB_2534069	IF: 1:250
Alexa Fluor 555 goat anti-rabbit IgG	ThermoFisher Scientific	A-32732	AB_2633281	IF: 1:250
Alexa Fluor 488 goat anti-rabbit IgG	ThermoFisher Scientific	A-11034	AB_2576217	IF: 1:250
Alexa Fluor 555 goat anti-mouse IgG	ThermoFisher Scientific	A-21424	AB_141780	IF: 1:250
Goat Biotinylated anti-Rabbit IgG (H&L)	Vector Laboratories	BA-1000	AB_2313606	IHC: 1:250
Oligonucleotides				
LRRK1 PCR Forward Primer for Left arm amplification: P1 5'-GACATCCGCGGCACCATGTGAGTGGCAGCTGTGGTGAGAAC-3' *Sac*II sequence is underlined.				
LRRK1 PCR Reverse Primer for Left arm amplification: P2 5'-GACATGCGGCCGCAAGCTTTTTAATAGCCGTTCTTTCTTAGAGAAGGCAG-3' *Not*I and *Hind*III sequences are underlined.				
LRRK1 PCR Forward Primer for Left-Middle arm amplification: P3 5'-CCAGTCACTTCTCCACCTCAGGGAAAATGG-3'				
LRRK1 PCR Reverse Primer for Left-Middle arm amplification: P4 5'-CCTTGTGGTACCCGGACCTTCTATCACCTTTATCC-3' *Kpn*I sequence is underlined.				
LRRK1 PCR Forward Primer for Right-Middle arm amplification: P5 5'-GGTCCGGGTACCACAAGGTGCTGGTTAAGTGCC-3' *Kpn*I sequence is underlined.				

LRRK1 PCR Reverse Primer for Right-Middle arm amplification: P6 5'-AGCAGACCTCTTGCCTTCTACTACTGACTG-3'
LRRK1 PCR Forward Primer for Right arm amplification: P7 5'- GACATGTCGACGGATCCGTAGGGAAGACCCACTAGGAGGAAGAAAG-3' *Sal*I sequence is underlined.
LRRK1 PCR Reverse Primer for Right arm amplification: P8 5'- GACATAAGCTTTGGTACCTTTCTAAAGGCAGCATTTTGCTTGC-3' *Hind*III sequence is underlined.
LRRK1 PCR Forward Primer for 5' Southern Probe: P15 5'-CAGAATACCCCATGCTGGGGAATTGC-3'
LRRK1 PCR Reverse Primer for 5' Southern Probe: P16 5'-CCGTTTCTAGGATTCTAATTTTTC-3'
LRRK1 PCR Forward Primer for 3' Southern Probe: P17 5'-AACTCCTTCCTGGTGCTGGCAGGCCTGGCTG-3'
LRRK1 PCR Reverse Primer for 3' Southern Probe: P18 5'-ACAAGTGACGTGACCATGGACGGAGCTGCG-3'
Neo PCR Forward Primer for Southern Probe: P23 5'-ATTCGGCTATGACTGGGCAC-3'
Neo PCR Reverse Primer for Southern Probe: P24 5'-GACCACCAAGCGAAACATCG-3'
LRRK1 PCR Forward Primer for exons 2-3 Northern Probe: P31 5'-CAGGATGAGCGTGTGTCTGCAG-3'
LRRK1 PCR Reverse Primer for exons 2-3 Northern Probe: P32 5'-CCTTCTCCTGTGAGGATTCGCTCT-3'
LRRK1 PCR Forward Primer for exons 27-29 Northern Probe: P33 5'-CTGGCCTACCTGCACAAGAA-3'
LRRK1 PCR Reverse Primer for exons 27-29 Northern Probe: P34 5'-CCTTCCCATCCCAGAACACC-3'
GADPH PCR Forward Primer for Northern Probe: P37 5'-ACCACAGTCCATGCCATCAC-3'
GADPH PCR Reverse Primer for Northern Probe: P38 5'-TCCACCACCCTGTTGCTGTA-3'
LRRK1 RT Primer in exons 32: P47 5'-GGCTCAGGTCATGCTCAGTT-3'
LRRK1 PCR Forward Primer for exons 4-8 RT-PCR: P53 5'-TTTTGGACACGCCGAAGTAGT-3'
LRRK1 PCR Reverse Primer for exons 4-8 RT-PCR: P54 5'-AGCCGCTCCAGGTAGTTTTT-3'
LRRK1 PCR Forward Primer for exons 11-17 RT-PCR: P57 5'-GGACCTCTCCAGAAACCAGC-3'
LRRK1 PCR Reverse Primer for exons 11-17 RT-PCR: P58 5'-GCAGGGTTGCTATCCTCTCC-3'
LRRK1 PCR Forward Primer for exons 20-25 RT-PCR: P63 5'-GCGGTCAGTGGCAAAGAATG-3'
LRRK1 PCR Reverse Primer for exons 20-25 RT-PCR: P64 5'-AATGCTGTTCTCACCCTCCG-3'
LRRK1 PCR Forward Primer for exons 25-31 RT-PCR: P41 5'-GAATTCTGCTAATGCCCCAGC-3'
LRRK1 PCR Reverse Primer for exons 25-31 RT-PCR: P42 5'-AGGCTGTAGATATAGATTTTCTGGT-3'

LRRK2 PCR Forward Primer for Left arm amplification: P9 5'-GAACACACAAGGCTATGGCTATTGTC-3'
LRRK2 PCR Reverse Primer for Left arm amplification: P10 5'-GTAGGACTATCATCCACCTGTAGGACTCC-3'
loxP site introducing oligo for *LRRK2*: P39 5'-GATCCATAACTTCGTATAATGTATGCTATACGAAGTTATGCTAGCA-3' *BamH*I and *Nhe*I sequences are underlined.
loxP site introducing oligo for *LRRK2*: P40 5'-CTAGTGCTAGCATAACTTCGTATAGCATACATTATACGAAGTTATG-3' *Spe*I and *Nhe*I sequences are underlined.
LRRK2 PCR Forward Primer for Middle arm amplification: P11 5'-GTCCTACAGGTGGATTCTAGACCTACAAGG-3' *Xba*I sequence is underlined.
LRRK2 PCR Reverse Primer for Middle arm amplification: P12 5'-GACGCGGCCGCGTTTAGTAGCTAGCATGACTATGAAGGAG-3' *Not*I and *Nhe*I sequences are underlined.
LRRK2 PCR Forward Primer for Right arm amplification: P13 5'-GCACTTGAGTCTTAATCTTGGGCAC-3'
LRRK2 PCR Reverse Primer for Right arm amplification: P14 5'-CATTCGAGCAGCTAAGCCTGTAATC-3'
LRRK2 PCR Forward Primer for 5' Southern Probe: P19 5'-CATGGGAGAGAGGGTTTCTCACTTACT-3'
LRRK2 PCR Reverse Primer for 5' Southern Probe: P20 5'-CTTGGACAGCATTGTCAGCCTAGAC-3'
LRRK2 PCR Forward Primer for 3' Southern Probe: P21 5'-GCCAAGCAGTTATTGATGCTGTAGC-3'
LRRK2 PCR Reverse Primer for 3' Southern Probe: P22 5'-CGAGCTGTAAGATGAGCTGGGTACT-3'
LRRK2 PCR Forward Primer for Northern Probe: P35 5'-AGGAAGGCAAGCAGATCGAG-3'
LRRK2 PCR Reverse Primer for Northern Probe: P36 5'-GGCTGAATATCTGTGCATGGC-3'
LRRK2 RT Primer in exons 51: P93 5'-TCGTGTGGAAGATTGAGGTCC-3'
LRRK1 PCR Forward Primer for Genotyping: P25 5'-ATTGGTCTTTGAAGAGACAGCATCTGG-3'
LRRK1 PCR Reverse Primer for Genotyping: P26 5'-TTTCCCTGAGGTGGAGAAGTGACTGG-3'
LRRK1 PCR Reverse Primer for Genotyping: P27 5'-TCACGTCGTCTAAGCCTCCT-3'
LRRK1 PCR Forward Primer for Genotyping: P28 5'-CTTCCTCAGAAGTTAGGTAAACATTG AGTG-3'
LRRK1 PCR Reverse Primer for Genotyping: P29 5'-CTAAGTGACACCGTGTTTCCAAAGTC-3'
LRRK1 PCR Reverse Primer for Genotyping: P30 5'-GGAAAGTTTCACAATTGGAAAAATAAAAATATTTACTGCAGATA-3'
DAT-IRES-Cre PCR Forward Primer for Genotyping: JKM1823 5'-TGGCTGTTGGTGTAAGTGG-3'
DAT-IRES-Cre PCR Reverse Primer for Genotyping: JKM1824 5'-GGACAGGGACATGGTTGACT-3'

DAT-IRES-Cre PCR Reverse Primer for Genotyping: JKM1825 5'-CCAAAGACGGCAATATGGT-3'

300

301 **Mice**

302 All animal use was approved by the IACUC committees of Harvard Medical School and Brigham
303 and Women's Hospital, and conformed to the USDA Animal Welfare Act, PHS Policy on Humane Care
304 and Use of Laboratory Animals, the "ILAR Guide for the Care and Use of Laboratory Animals" and other
305 applicable laws and regulations. Mice were housed in constant humidity- and temperature-controlled
306 rooms and maintained on a 12 hr light/dark cycle and were given standard rodent chow and water. Mice
307 of both sexes at multiple ages, from 2 months to 25 months, were used. Floxed *LRRK1* (*fLRRK1*) and the
308 resulting germline deleted *LRRK1*$^{\Delta}$ alleles, and floxed *LRRK2* (*fLRRK2*) and the resulting germline
309 deleted *LRRK2*$^{\Delta}$ alleles were generated and thoroughly validated at the genomic DNA, mRNA, and
310 protein levels. *DAT-IRES-Cre* (The Jackson Laboratory, IMSR_JAX:006660), *ACT-FLPe*
311 (IMSR_JAX:005703), *CMV-Cre* transgenic (IMSR_JAX:006054), and *Rosa26-CAG-LSL-ZsGreen1* mice
312 (IMSR_JAX:007906) used in the current study were previously characterized and reported (32-35).
313 *LRRK1/LRRK2* cDKO mice (*fLRRK1/fLRRK1; fLRRK2/fLRRK2; DAT-IRES-Cre/+*) and littermate
314 controls (*fLRRK1/fLRRK1; fLRRK2/fLRRK2*) were obtained from multiple breeding cages of
315 *fLRRK1/fLRRK1; fLRRK2/fLRRK2* and cDKO mice. All mice were maintained on the C57BL6 and 129
316 hybrid genetic background (F1: IMSR_JAX:101043). All phenotypic analyses were performed in a
317 genotype blind manner, as previously described (67).

318 **Generation of targeted and floxed *LRRK1* and *LRRK2* alleles**

319 The generation and validation of the *LRRK1* and *LRRK2* targeting vectors, the targeted, floxed,
320 and deleted *LRRK1* and *LRRK2* alleles by Southern, Northern, RT-PCR, and the sequences of the floxed
321 *LRRK1* and *LRRK2* alleles are included in Figure 1-figure supplement 1-11.

322 ***LRRK1***

323 To generate the *LRRK1* targeting vector, we first PCR amplified the *left middle* homologous
324 region (2,079 bp) containing partial intron 26, exon 27, and partial intron 27 of *LRRK1* from mouse BAC
325 DNA (clone RP23-213J23, BACPAC Resources Center) using primers, P3 and P4. The PCR fragment
326 was subcloned into the *pGEM-T* vector (A1360, Promega) to generate pLM1 (for details, see Figure 1-
327 figure supplement 1). The *right middle* homologous region (3,403) containing *LRRK1* genomic region
328 from partial intron 27 to partial intron 29 was amplified by PCR using primers, P5 and P6, and then
329 subcloned into the *pGEM-T* vector (pLM2). The *left middle* homologous region containing *pGEM-T*
330 plasmid was then digested with *Not*I and *Kpn*I (endogenous *Kpn*I site in the intron 27) and subcloned into
331 the *Not*I and *Kpn*I sites of the *right middle* homologous region containing *pGEM-T* plasmid (pLM3).
332 After that, the *middle* homologous region (5.5 kb), from partial intron 26 to partial intron 29, was released
333 by *Not*I and *Sac*II digestions and was blunted by Klenow, and then subcloned into the *Sma*I site of
334 *PGKneoF2L2DTA* vector (#13445, addgene) to generate the *middle* homologous region-
335 *PGKneoF2L2DTA* plasmid (pLM4).

336 The *left* homologous region (2,016 bp) containing partial intron 25, exon 26, and partial intron 27
337 of *LRRK1* was PCR amplified from mouse BAC DNA (clone RP23-213J23, BACPAC Resources Center)
338 using primers, P1 and P2. The PCR fragment was digested with *Sac*II (introduced by P1) and *Not*I
339 (introduced by P2 along with *Hind*III), and was subcloned into the *Sac*II and *Not*I sites of the
340 *PGKneoF2L2DTA* vector (pLM5). The *right* homologous region (3,131 bp) containing partial intron 29,
341 exon 30, and partial intron 30 of *LRRK1* was PCR amplified from mouse BAC DNA (clone RP23-213J23)
342 using primers, P7 and P8. The PCR fragment was digested with *Sal*I (introduced by P7) and *Hind*III
343 (introduced by P8), and was subcloned into the *Sal*I and *Hind*III sites of the *PGKneoF2L2DTA* vector
344 (pLM6).

345 The *left* homologous region in the *PGKneoF2L2DAT* vector (pLM5) was digested with *Sac*II and
346 *Not*I, and subcloned into the *Sac*II and *Not*I sites of the *right* homologous region containing
347 *pGKneoF2L2DTA* plasmid (pLM6) to generate pLM7. Finally, the *loxP-middle* homologous region-*PGK-*
348 *Neo-loxP* fragment was released from pLM4 by *Not*I and *Sal*I digestions, and subcloned into the *Not*I and

349 *Sal*I sites of pLM7 to generate the final target vector (pLM8), which contains two *loxP* sites (intron 26
350 and intron 29). Upon Cre-mediated recombination, the endogenous *LRRK1* genomic sequence flanked by
351 the 5' *loxP* site (1,288 bp upstream of *LRRK1* exon 27) to the 3' *loxP* site (1,023 bp downstream of exon
352 29) is excised. The *PGK-neo* cassette flanked by two *FRT* sites is under the control of the mouse
353 *phosphoglycerate kinase 1* (*PGK*) promoter and contains the *bovine growth hormone* polyA signal. To
354 enhance the ratio of ES cells carrying homologous recombination events instead of random insertion of
355 the targeting vector (68), the negative selection *PGK-DTA* cassette, which encodes diphtheria toxin A
356 chain, was also included in the *LRRK1* targeting vector.

357 The *LRRK1* targeting vector was linearized by *Xho*I digestion, and then electroporated into
358 MKV6.5 embryonic stem (ES) cells (a gift from R. Jaenisch), which were derived from B6/129 F1 mice
359 (The Jackson Laboratory, IMSR_JAX:101043). G418 was applied to the culture at 150 μg/ml 24 h later,
360 and after 6 days of G418 selection, the surviving ES clones (480) were picked and screened by Southern
361 analysis using *Hind*III digestion of genomic DNA followed by hybridization with the 5' external and 3'
362 external probes to confirm proper recombination events in the 5' and 3' homologous regions, respectively.
363 25 ES cell clones were confirmed to carry the proper homologous recombination events at the 5'
364 homologous region, giving rise to the 17.0 kb and the 4.8 kb bands, which represent the wild-type and the
365 targeted allele, respectively (Figure 1D), and the 3' homologous region, giving rise to the 17.0 kb and the
366 14.1 kb bands, which represent the wild-type and the targeted allele, respectively. We then expanded the
367 selected 4 ES cell clones (3A11, 3D8, 3H1, and 3H6) and further verified by Southern using the 5' and 3'
368 external, and *neo* probes. Two ES cell clones (3D8 and 3H6) were transfected with *pCAGGS-flpE-puro*
369 (#20733, addgene) to delete the *PGK-neo* cassette by FLP recombinase. Three resulting ES cell clones
370 (3D8C5, 3D8E5, and 3H6G7) were confirmed by Southern analysis using the 5' and 3' external probes
371 and the *neo* probe to confirm the floxed *LRRK1* allele by the deletion of the *PGK-neo* cassette.

372 ***LRRK2***

373 To generate the *LRRK2* targeting vector, the *left* homologous region (2,579 bp) containing the
374 *LRRK2* promoter region was PCR amplified from mouse BAC DNA (clone RP23-526A2, BACPAC
375 Resources Center) using primers, P9 and P10, and subcloned into the *pGEM-T* vector to generate
376 pLRRK2#1 (for details see Figure 1-figure supplement 4). The *BamH*I-*loxP*-*Nhe*I-*Spe*I fragment (56 bp),
377 which was generated by annealing two complementary oligos, P39 and P40, was introduced to the *BamH*I
378 and *Spe*I sites of pLRRK2#1 to generate pLRRK2#2. The *middle* homologous region, containing genomic
379 sequences from the promoter region to partial intron 2, was PCR amplified from mouse BAC DNA (clone
380 RP23-526A2) using primers, P11 and P12, digested with *Xba*I and *Not*I, and subcloned into the *Xba*I and
381 *Not*I sites of the *pGEM-T* vector to generate pLRRK2#3, which was digested with *Xba*I and *Not*I, and
382 subcloned into the *Xba*I and *Not*I sites of pLRRK2#2 to generate pLRRK2#4.
383 The *right* homologous region (3,503 bp), which contains partial intron 1, exon 2, and partial
384 intron 2, was PCR amplified from mouse BAC DNA (clone RP23-526A2) using primers, P13 and P14,
385 and the PCR fragment was subcloned into the *EcoR*V site of *pBluescript II KS* (+) vector (212207,
386 Agilent) to generate pLRRK2#5. The *right* homologous region in pLRRK2#5 was digested with *BamH*I
387 followed by Klenow, and then digested with *Cla*I. The released fragment was subcloned into the *EcoR*V
388 and *Cla*I sites of the *PGKneoF2L2DTA* vector to generate pLRRK2#6. *LFNT-tk/pBS* plasmid (a gift from
389 S. Tonegawa) was digested with *Sac*II (followed by Klenow) and *Not*I (followed by *Ssp*I digestion to
390 make it easier to isolate the *Not*I-*Sac*II/KN fragment) to release the *loxP-FRT-PKG-neo-loxP-FRT*
391 fragment (2,928 bp), and then subcloned into the *Xba*I (followed by Klenow) and *Not*I sites of
392 pLRRK2#6 to generate pLRRK2#7. Finally, pLRRK2#4 containing the *left-loxP-middle* homologous
393 regions was digested with *EcoR*V and *Not*I, and subcloned into *Ale*I and *Not*I sites of pLRRK2#7
394 containing the *loxP-FRT-PKG-neo- loxP-FRT-right* homologous region to generate the final targeting
395 vector, which contains the *loxP* sites in the promoter region (1,768 bp upstream of the transcription
396 initiation site) and in *LRRK2* intron 2 (878 bp downstream of exon 2). Upon Cre-mediated recombination,
397 the floxed endogenous *LRRK2* genomic sequences from the 5' *loxP* site (1,768 bp upstream of *LRRK2*

398 transcription) to the 3' *loxP* site in intron 2 (878 bp downstream of exon 2) are excised. The negative
399 selection *PGK-DTA* cassette is also included in the *LRRK2* targeting vector.

400 The *LRRK2* targeting vector was linearized by *Ahd*I digestion, and then electroporated into
401 MKV6.5 ES cells. G418 was applied to the culture at 150 ug/ml 24 h later, and after 6 days of G418
402 selection, the surviving ES clones (480) were picked and screened by Southern analysis using *Nhe*I
403 digestion of genomic DNA followed by hybridization with the 5' external probe (753 bp, PCR amplified
404 using P19 and P20). Southern analysis confirmed that two ES cell clones (N24 and N34) carry the proper
405 recombination event in the 5' homologous arm, giving rise to 11.6 kb and 3.6 kb bands, which represent
406 the wild-type and targeted alleles, respectively (Figure 1F), followed by genomic PCR confirmation for
407 the proper recombination in the right arm.

408 Three (3D8C5, 3A11, 3H6) and one (N24) ES clones for *LRRK1* and *LRRK2*, respectively, were
409 microinjected into C57BL/6 mouse blastocysts to generate chimera mice, which were bred with B6/129
410 F1 mice to produce heterozygous floxed *LRRK1* and targeted *LRRK2* mice. Floxed *LRRK1* mice were
411 confirmed by Southern analysis using the 5' and 3' external probes (Figure 1D). Targeted *LRRK2* mice
412 were confirmed by Southern (data shown in Figure 1-figure supplement 6; *Nhe*I digestion followed by
413 hybridization with the 5' external probe and *Sph*I digestion followed by hybridization with the 3' external
414 probe). Targeted *LRRK2* mice were then bred with *Actin-FLP* deleter mice (IMSR_JAX:005703) (33) to
415 generate floxed *LRRK2* mice, which were confirmed by Southern analysis using the 5' and 3' external
416 probes following *Nhe*I digestion (Figure 1F). Heterozygous *fLRRK1*/+ and *fLRRK2*/+ mice were crossed
417 with each other to obtain homozygous single floxed mice (*fLRRK1/fLRRK1* and *fLRRK2*/*fLRRK2*) and
418 double floxed mice (*fLRRK1/fLRRK1*; *fLRRK2*/*fLRRK2*).

419 **Generation of deleted *LRRK1/LRRK2* alleles and DA neuron-specific cDKO mice**

420 In order to ensure that Cre-mediated deletion of the floxed *LRRK1* and *LRRK2* alleles results in
421 null alleles, we crossed floxed *LRRK1* and *LRRK2* mice with germline deleter, *CMV-Cre* transgenic mice
422 (*B6.C-Tg(CMV-cre)1Cgn/J*; IMSR_JAX:006054) (34), to generate *LRRK1* deleted (Δ/Δ) mice (by

423 removing exons 27-29) and *LRRK2* deleted (Δ/Δ) mice (by removing the promoter region and exons 1-2)
424 for further molecular characterization. To generate DA neuron-specific *LRRK1*/*LRRK2* cDKO mice, we
425 used *DAT-Cre* KI mice (*B6.SJL-Slc6a3tm1.1(cre)Bkmn/J;* IMSR_JAX:006660), which express Cre
426 recombinase under the control of the endogenous *DAT* promoter (32). We crossed double floxed mice
427 with *DAT-Cre* mice to generate *LRRK* cDKO mice (*fLRRK1*/*fLRRK1; fLRRK2*/*fLRRK2*; *DAT-Cre/+*).
428 *LRRK* cDKO and littermate control mice used in the phenotypic analysis were obtained by crossing
429 *fLRRK1*/*fLRRK1; fLRRK2*/*fLRRK2; DAT-Cre/+* with *fLRRK1*/*fLRRK1; fLRRK2*/*fLRRK2* mice. We only
430 used cDKO and control mice that carry all floxed *LRRK1* and *LRRK2* alleles for phenotypic analysis.

431 **Southern analysis**

432 For the identification and validation of the targeted and floxed *LRRK1* alleles, we used the 5'
433 external, 3' external, and *neo* probes. Genomic DNA from ES cells or mouse tails was digested with
434 *Hind*III. The 5' external probe (377 bp), which is 839 bp upstream of the 5' homologous region, was PCR
435 amplified from mouse BAC DNA (clone RP23-213J23) using primers P15 and P16. The 3' external
436 probe (305 bp), which is 2,736 bp downstream of the 3' homologous region, was PCR amplified from
437 mouse BAC DNA (clone RP23-213J23) using primers P17 and P18. The *neo* probe (363 bp) was PCR
438 amplified from pSoriano plasmid using primers P23 and P24. Following *Hind*III digestion, the presence
439 of the 17.0 kb product using either the 5' or 3' external probe represents the wild-type allele, whereas the
440 4.8 kb (the 5' external probe) and the 12.2 kb (the 3' external probe) products represent the floxed *LRRK1*
441 allele. Genomic DNA digested by *Hind*III and hybridized with the *neo* probe further confirmed the wild-
442 type and floxed alleles (no band) and the targeted *LRRK1* allele (14.1 kb).

443 For the identification and validation of the targeted and floxed *LRRK2* alleles, we used the 5' and
444 3' external probes as well as the *neo* probe. Genomic DNA from ES cells or mouse tails was digested
445 with *Nhe*I or *Sph*I followed by hybridization with the 5' or 3' external probe or the *neo* probe. The 5'
446 external probe (753 bp), which is 84 bp upstream of the 5' homologous region, was PCR amplified from
447 mouse BAC DNA (clone RP23-526A2) using primers P19 and P20. The 3' external probe (622 bp),

448 which is 38 bp downstream of the 3' homologous region, was PCR amplified from mouse BAC DNA
449 (clone RP23-526A2) using primers P21 and P22. Following *Nhe*I digestion, the presence of the 11.5 kb
450 product using either the 5' or 3' external probe represents the wild-type allele, whereas the 3.6 kb (the 5'
451 external probe) and the 5.2 kb (the 3' external probe) products represent the floxed *LRRK2* allele.

452 **PCR genotyping**

453 Genomic PCR was performed to determine the presence of the deleted, the floxed, and/or the
454 wild-type alleles. For *LRRK1*, the following primers were used: P25 (5'-
455 ATTGGTCTTTGAAGAGACAGCATCTGG, forward primer, 392 nt downstream of exon 26), P26 (5'-
456 TTTCCCTGAGGTGGAGAAGTGACTGG, reverse primer, 567 nt downstream of exon 26), and P27
457 (5'-TCACGTCGTCTAAGCCTCCT, reverse primer, 1,218 nt downstream of exon 29). The PCR
458 products from P25 and P26 are 266 bp and 405 bp, which represent the wild-type and the *fLRRK1* alleles,
459 respectively, whereas the PCR product from P25 and P27 is 583 bp, which represents the deleted *LRRK1*
460 allele.

461 For *LRRK2*, the following primers were used: P28 (5'-
462 CTTCCTCAGAAGTTAGGTAAACATTGAGTG, forward primer, 2,069 nt upstream of exon 1), P29
463 (5'-CTAAGTGACACCGTGTTTCCAAAGTC, reverse primer, 1,739 nt upstream of exon 1), and P30
464 (5'-GGAAAGTTTCACAATTGGAAAAATAAAAATATTTACTGCAGATA, reverse primer at 2,848 nt
465 downstream of exon 2). The PCR products from P28 and P29 are 305 bp and 367 bp, representing the
466 wild-type and the *fLRRK2* alleles, respectively, whereas the PCR product from P28 and P30 is 587 bp,
467 which represents the deleted *LRRK2* allele.

468 For *DAT-IRES-Cre*, the following primers were used: JKM1823 (5'-
469 TGGCTGTTGGTGTAAAGTGG, forward primer at exon 16 and 3'-UTR), JKM1824 (5'-
470 GGACAGGGACATGGTTGACT, reverse primer at 3'-UTR), and JKM1825 (5'-
471 CCAAAAGACGGCAATATGGT, reverse primer at *IRES* sequence). The PCR product from JKM1823

472 and JKM1824 is 264 bp, which represents the wild-type allele, whereas the PCR product from JKM1823
473 and JKM1825 is 152 bp, which represents the *DAT-IRES-Cre* KI allele.

474 **Northern analysis**

475 Total RNA was isolated from brains, kidneys, or lungs using TRI reagent (T9424, Millipore-
476 Sigma) according to the manufacturer's instruction. For the *LRRK1* Northern analysis, polyA+ RNA was
477 enriched from ~500 μg total RNA using the Poly(A)Purist™ MAG Kit (AM1922, ThermoFisher)
478 according to the manufacturer's instruction. For the *LRRK2*, ~10 μg of total RNA was used for Northern
479 analysis. RNA was separated in formaldehyde agarose gel, and transferred into Amersham Hybond-nylon
480 membrane (RPN303N, GE Healthcare). Probes were synthesized using Prime-It II random labeling kit
481 (#300385, Agilent) and then used for membrane hybridization at 55ºC overnight.

482 The cDNA probe specific for *LRRK1* exons 2-3 (383 bp) was PCR amplified using primers P31
483 (5'-CAGGATGAGCGTGTGTCTGCAG) and P32 (5'-CCTTCTCCTGTGAGGATTCGCTCT). The
484 cDNA probe specific for *LRRK1* exons 27-29 (550 bp) was PCR amplified using primers P33 (5'-
485 CTGGCCTACCTGCACAAGAA) and P34 (5'-CCTTCCCATCCCAGAACACC).

486 The cDNA probe specific for *LRRK2* exons 1-5 (437 bp) was PCR amplified using primers P35
487 (5'-AGGAAGGCAAGCAGATCGAG) and P36 (5'-GGCTGAATATCTGTGCATGGC). The probe
488 specific for *GAPDH* exons 5-7 (452 bp) was PCR amplified using primers P37 (5'-
489 ACCACAGTCCATGCCATCAC) and P38 (5'-TCCACCACCCTGTTGCTGTA).

490 Hybridization was performed using α-^{32}P-dCTP-labeled probes specific to each gene. Specific
491 signals were detected by autoradiography with Hyperfilm (E3018, Amersham).

492 **RT-PCR**

493 Total RNA was isolated from brains, kidneys, or lungs using TRI reagent (T9424, Millipore-
494 Sigma) according to the manufacturer's instruction. Approximately 1 μg of RNA was reverse-transcribed
495 using Superscript III (18080093, Thermo Fisher Scientific) according to the manufacturer's instructions.
496 For RT-PCR analysis of *LRRK1* transcripts in mice carrying the homozygous floxed or deleted alleles, we

497 used primers P53 and P54 for exons 4-8 (714 bp), P57 and P58 for exons 11-17 (818 bp), P63 and P64 for
498 exons 20-25 (922 bp), or P41 and P42 for exons 25-31 to confirm normal splicing of *LRRK1* mRNA in
499 *fLRRK1/fLRRK1* mice and truncated *LRRK1* transcripts lacking exons 27-29 in Δ/Δ mice (for details see
500 Figure 1-figure supplement 9). For RT-PCR analysis of *LRRK2* transcripts, we used primers P35 and P36
501 in exons 1-5 to confirm normal splicing of *LRRK2* mRNA (437 bp) in *fLRRK2/fLRRK2* mice and the
502 absence of RT-PCR products in *LRRK2* Δ/Δ mice (Figure 1-figure supplement 11). The identity of the
503 PCR products was confirmed by sequencing.

504 **Western analysis**

505 Fresh tissues were collected and homogenized in an ice-cold stringent RIPA buffer (50 mM Tris-
506 Cl (pH 7.6), 150 mM NaCl, 0.5 mM EDTA, 1% NP40, 0.5% sodium deoxycholate, 0.1% SDS, 1mM
507 PMSF supplement with protease inhibitor cocktail (P8340, Sigma) and phosphatase inhibitor cocktail
508 (P0044, Sigma)), followed by sonication. Homogenates were centrifuged at 14,000xg for 20 min at 4ºC to
509 separate supernatants (RIPA buffer-soluble fraction). An equal amount (10-40 μg per lane) of total
510 proteins from each preparation were loaded and separated on NuPAGE gels (Invitrogen), and transferred
511 to nitrocellulose membranes. The membranes were blocked in Intercept (TBS) Blocking Buffer (927-
512 60001, Li-Cor) for 1 hr at room temperature, and incubated at 4ºC overnight with specific primary
513 antibodies. Primary antibodies used were rabbit anti-LRRK1 (ANR-101, Alomone Lab, RRID:
514 AB_2756700), rabbit anti-LRRK2 (ab133474, abcam, RRID: AB_2713963), mouse anti-α-Vinculin (05-
515 386, Millipore, RRID: AB_309711). Membranes were then incubated with dye-coupled secondary
516 antibodies, goat anti-mouse IRdye680 (#925-68070, LI-COR, RRID: AB_2651128) or goat anti-rabbit
517 IRdye800 (#925-32211, LI-COR, RRID: AB_2651127). Signals were quantified using the Odyssey
518 Infrared Imaging System (LI-COR).

519 **Histological analysis**

520 Mice were anesthetized with ketamine (100 mg/kg) + xylazine (10 mg/kg) + acepromazine (3
521 mg/kg), and transcardially perfused with phosphate-buffered saline solution (PBS, pH 7.4) containing

522 0.25 g/L heparin (H3149, Sigma) and 5 g/L procaine (P9879, Sigma). Brains were post-fixed in 4%
523 formaldehyde in PBS (pH 7.4) (15710, Electron Microscopy Sciences) at 4˚C overnight and then
524 processed for paraffin embedding following standard procedures. For frozen sections, post-fixed brains
525 were immersed in a sucrose series solution (15% and 30% sucrose in PBS) at 4ºC overnight for
526 cryoprotection, and then brains were embedded in an OCT compound (4583, Sakura). Serial coronal
527 sections (16 μm) of paraffinized brains or frozen brains were obtained using Leica RM2235 or Leica
528 CM1860, respectively. Coronal sections containing the SNpc or LC were selected for
529 immunohistochemical analysis.

530 Histological analyses were performed as described previously (30, 31, 67). Briefly, for DAB-
531 derived TH-immunohistochemistry, coronal sections were deparaffinized, alcohol-dehydrated, and then
532 subjected to permeabilization with a solution containing 0.1% Triton X-100 in TBS followed by antigen
533 retrieval for 5 min in 10 mM sodium citrate buffer, pH 6.0. Endogenous peroxidase activity was quenched
534 by incubating in 0.3% H_2O_2 in methanol. Sections were then blocked with a solution containing 5%
535 normal goat serum (S-1000, Vector Laboratories) and 0.1% Triton X-100 in TBS for 1 hr at room
536 temperature. After blocking, sections were incubated with the primary antibody, rabbit anti-TH (1:750,
537 ab112, abcam, RRID: AB_297840) overnight at 4ºC. Sections were washed three times in 0.1% Triton X-
538 100 in TBS followed by 1 hr incubation with goat biotinylated anti-rabbit IgG secondary antibody (1:250,
539 BA-1000, Vector Laboratories, RRID: AB_2313606) at room temperature and 30 min incubation with
540 Vectastain Elite ABC reagent (PK-6100, Vector Laboratories) and then developed using chromogenic
541 DAB substrate (SK-4100, Vector Laboratories).

542 For immunofluorescence staining of paraffin sections, coronal sections were deparaffinized,
543 alcohol-dehydrated, and then subjected to permeabilization with a solution containing 0.1% Triton X-100
544 in PBS followed by antigen retrieval for 5 min in 10 mM sodium citrate buffer, pH 6.0 except those for
545 cleaved-caspase3 immunostaining which were performed antigen retrieval for 10 min. Sections were then
546 blocked with a solution containing 10% normal goat serum and 0.1% Triton X-100 in PBS for 1 hr at
547 room temperature. After blocking, sections were incubated with primary antibodies overnight at 4ºC. The

548 primary antibodies used were mouse anti-TH (1:50, sc-25269, Santa Cruz, RRID: AB_628422), rabbit
549 anti-NeuN (1:400, 12943S, Cell Signaling Technology, RRID: AB_2630395), rabbit anti-cleaved
550 caspases-3 (1:150, 9661, Cell Signaling Technology, RRID: AB_2341188), or rabbit anti-Iba1 (1:500,
551 019-19,751, Wako, RRID: AB_839504). Sections were washed three times in 0.1% Triton X-100 in PBS
552 followed by 1 hr incubation with fluorophore-conjugated secondary antibodies, goat anti-mouse IgG
553 Alexa Fluor 488 (1:500, A11001, ThermoFisher, RRID: AB_2534069) and goat anti-rabbit IgG Alexa
554 Fluor 555 (1:500, A32732, ThermoFisher, RRID: AB_2633281) at room temperature. Fluorescence
555 images were taken (a stack of 2-3 confocal images spaced at 4 μm), projected with maximal intensity
556 projection mode, and analyzed by FV1000 confocal microscope system (Olympus)

557 For immunofluorescence staining of cryopreserved sections, coronal brain sections were washed
558 with PBS to rinse out OCT, and then blocked with a solution containing 5% normal goat serum and 0.1%
559 Triton X-100 in TBS for 1 hr at room temperature. After blocking with 10% NGS, sections were
560 incubated with primary antibodies, rabbit anti-GFP (1: 1000, ab290, abcam, RRID: AB_303395), and
561 mouse anti-TH (1:50, sc-25269, Santa Cruz, RRID: AB_628422), overnight at 4ºC. Sections were
562 incubated with fluorophore-conjugated secondary antibodies, goat anti-rabbit IgG Alexa Fluor 488 (1:500,
563 A11034, ThermoFisher, RRID: AB_2576217) and goat anti-mouse IgG Alexa Fluor 555 (1:250, A21424,
564 ThermoFisher, RRID: AB_141780) for 1 hr at room temperature. Fluorescence images were taken and
565 analyzed by FV1000 confocal microscope system (Olympus).

566 The number of GFP+ and GFP+/TH+ cells in the SNpc of *DAT-IRES-Cre/+; Rosa26-CAG-LSL-*
567 *ZsGreen1/+* reporter mice were quantified using 3 comparable coronal sections (16 μm in thickness,
568 spaced 320 μm apart) per brain (n = 3 brains, one hemisphere). The percentage of GFP+ DA neurons in
569 the SNpc was obtained by dividing the sum of GPF+/TH+ neurons by the sum of total TH+ neurons
570 quantified.

571 Quantification of TH+ DA neurons in the SNpc or LC was performed as previously described (30,
572 31, 67, 69). Briefly, TH+ neurons in the SNpc, which were marked based on morphological features as

573 previously described (70), were quantified in every 10th serial coronal section (16 μm in thickness)
574 throughout the SNpc (a total of 6-9 sections, spaced 160 μm apart). Total number of TH+ cells in the
575 SNpc was calculated as follows: [total number of TH+ DA neurons quantified in all 6-9 sections] x 10
576 (every 10th section sampled) x 2 (both hemispheres). Similar results were obtained independently by two
577 investigators using coded samples. Total number of TH+ noradrenergic neurons in the LC (a total of 6-9
578 sections, spaced 80 μm apart) was calculated as follows: [total number of TH+ noradrenergic neurons
579 quantified in all 6-9 sections] x 5 (every 5th section sampled) x 2 (both hemispheres).

580 NeuN+, active Caspase-3+, or Iba1+ cells in the SNpc, which was marked by TH
581 immunoreactivity, were quantified using serial coronal sections (16 μm in thickness, every 10th section, a
582 total of 6-9 sections per brain). Compared to chromogenic DAB immunostaining followed by counting
583 under the stereomicroscope, which captures TH-positive dopaminergic neurons from the single plane
584 layer of the sections, immunofluorescence immunostaining picks up more cells with higher sensitivity by
585 maximal intensity projection mode throughout the entire layer of the section under the confocal
586 microscope. Thus, more TH-positive dopaminergic neurons in the SNpc were captured and quantified
587 under confocal microscopy compared to DAB staining. The total number of NeuN+, active Caspase-3+,
588 or Iba1+ cells in the SNpc, which was marked by TH immunoreactivity, was calculated as follows: [total
589 number of NeuN+, active Caspase-3+, or Iba1+ cells in all sections counted] x 10 (every 10th section
590 sampled) x 2 (both hemispheres).

591 **Quantitative EM analysis**

592 The collection and quantification of the EM images were performed as described previously (30,
593 71). Mice were perfused with PBS containing 0.25 g/L heparin and 5 g/L procaine followed by a fixative
594 solution containing 2.5% paraformaldehyde and 2.5% glutaraldehyde in 0.1 M sodium cacodylate buffer
595 (pH 7.4) (#1549, Electron Microscopy Science). Brains were dissected and post-fixed overnight in a
596 fixative solution at 4ºC. The dissected tissues were trimmed to 1-2 mm^3 cubes followed by osmication
597 and uranyl acetate staining, dehydration in graded alcohol, and embedded in TABB 812 Resin (Marivac

598 Ltd.) at the Harvard Medical School EM facility. 0.5 μm sections were stained with toluidine blue and
599 viewed under the light stereomicroscope (Nikon Eclips E600) to find the SNpc area for EM viewing.
600 Then adjacent sections were cut with 80 nm in thickness with the Leica Ultracut S microtome, picked up
601 on formvar-carbon coated slot Copper grids, stained with 0.2% Lead Citrate, and viewed and imaged
602 under the JEOL 1200x Electron Microscope. A minimum of 10 micrographs containing the entire cell
603 body in the SNpc area were analyzed for each brain. The image was analyzed by using the Fiji version of
604 ImageJ. The number of electron-dense autophagic and lysosomal vacuoles (> 0.5 μm in diameter) in
605 individual neuronal profiles was quantified. We previously calculated the diameter of electron-dense
606 autophagic/lysosomal vacuoles by measuring the longest side manually (30, 31). In the current study, we
607 used Feret's Diameter (72) to accurately measure the longest distance between any of two points in the
608 electron-dense autophagic/lysosomal vacuoles, resulting in a higher number of electron-dense vacuoles
609 quantified. The number of electron-dense vacuoles (> 0.5 μm in diameter) in individual neuronal profiles
610 was quantified. The area of electron-dense vacuoles (> 0.5 μm in diameter) was quantified and averaged
611 in individual neuronal profiles. Finally, the average number or area of vacuoles was calculated per
612 genotype. Experiments were done in a genotype blind manner (after scarifying mice, the brain samples
613 were coded and sent to the Harvard Medical School EM Core, where the images were captured, and the
614 vacuoles were quantified by another independent experimenter).

615 **Experimental design and statistical analysis**

616 Group sizes were determined based on prior studies. Littermates of control and cDKO mice were
617 randomly distributed between experimental groups. Data acquisition and quantification were performed in
618 a genotype blind manner with the exception of molecular analyses (Southern, Northern, RT-PCR, and
619 Western). All statistical analyses were performed using Prism 9 (GraphPad software) or Excel (Microsoft).
620 All data are presented as the means ± SEM. The exact sample size, the number of mice or neurons, of
621 each experiment is indicated in the figure or the legend.

622 Statistical analyses were conducted using a two-tailed Student's *t*-test for the comparison of a
623 given variable in two genotypes or two-way ANOVA followed by Bonferroni's post hoc comparisons for
624 the comparison of more than two conditions. Statistical outliers were identified and excluded using the
625 ROUT method with 1% the maximum desired false discovery rate developed by Prism. All statistical
626 comparisons were performed on data from ≥ 4 biologically independent samples and replicated on
627 different experimental days. Significance is shown as *$p < 0.05$, **$p < 0.01$, ***$p < 0.001$, ****$p <$
628 0.0001, and not significantly different values are often not noted.

629 **Data availability**

630 All data generated or analyzed during this study are included in the manuscript and supporting
631 file. Source Data files have been provided for Figures 1 to 7.

632 **Funding disclosure**

633 This work was supported by a grant from the NIH (R37NS071251 to J.S.).

634 **Acknowledgments**

635 We thank H. Zhao for technical assistance, Y. Yuan for organizing experimental data, and Shen
636 lab members for discussion. We are grateful to M. Ericsson at the Harvard Medical School Electron
637 Microscopy Core for her expert assistance.

638 **Author Contributions**

639 J.S. conceived and directed the project, J.K. performed Western blotting and quantitative
640 histological and EM analyses of *LRRK* cDKO mice (Figures 1I, 2E, F, 3, 4, 5A, B, 6, 7), G.H. performed
641 Northern blotting and RT-PCR followed by sequencing on mice carrying the floxed and deleted *LRRK1*
642 and *LRRK2* alleles (Figure 1G, H; Figure 1-figure supplement 8-11), preparation of brain sections and
643 histological analysis of TH+ neurons in *LRRK* cDKO mice at all ages (Figure 3A), J.K. and G.H. verified
644 all molecular results and compiled Figure 1-figure supplement 1, 2, 4, 5, L.M. (LRRK1) and Y.T.
645 (LRRK2) generated the targeting vectors and performed ES cell experiments including Southern blotting

646 (Figure 1C-F; Figure 1-figure supplement 1-6), P.C. performed GFP reporter analysis of *DAT-Cre* mice in
647 the SNpc (Figure 2A, B) and the LC (Figure 5C), J.K., G.H., P.C. analyzed the data and made the figures,
648 J.K., G.H., and J.S. wrote the paper.
649

650 **References**

651 1. Paisán-Ruíz C, Jain S, Evans EW, Gilks WP, Simón J, van der Brug M, et al. Cloning of the gene
652 containing mutations that cause PARK8-linked Parkinson's disease. Neuron. 2004;44(4):595-600.
653 2. Shen J. Protein kinases linked to the pathogenesis of Parkinson's disease. Neuron.
654 2004;44(4):575-7.
655 3. Zimprich A, Biskup S, Leitner P, Lichtner P, Farrer M, Lincoln S, et al. Mutations in LRRK2
656 cause autosomal-dominant parkinsonism with pleomorphic pathology. Neuron. 2004;44(4):601-7.
657 4. Gilks WP, Abou-Sleiman PM, Gandhi S, Jain S, Singleton A, Lees AJ, et al. A common LRRK2
658 mutation in idiopathic Parkinson's disease. Lancet. 2005;365(9457):415-6.
659 5. Lesage S, Janin S, Lohmann E, Leutenegger AL, Leclere L, Viallet F, et al. LRRK2 exon 41
660 mutations in sporadic Parkinson disease in Europeans. Arch Neurol. 2007;64(3):425-30.
661 6. Kluss JH, Mamais A, Cookson MR. LRRK2 links genetic and sporadic Parkinson's disease.
662 Biochem Soc Trans. 2019;47:651-61.
663 7. Shu L, Zhang Y, Sun Q, Pan H, Tang B. A Comprehensive Analysis of Population Differences in
664 LRRK2 Variant Distribution in Parkinson's Disease. Front Aging Neurosci. 2019;11:13.
665 8. Mata IF, Kachergus JM, Taylor JP, Lincoln S, Aasly J, Lynch T, et al. LRRK2 pathogenic
666 substitutions in Parkinson's disease. Neurogenetics. 2005;6(4):171-7.
667 9. Mata IF, Taylor JP, Kachergus J, Hulihan M, Huerta C, Lahoz C, et al. LRRK2 R1441G in
668 Spanish patients with Parkinson's disease. Neurosci Lett. 2005;382(3):309-11.
669 10. Zabetian CP, Samii A, Mosley AD, Roberts JW, Leis BC, Yearout D, et al. A clinic-based study of
670 the LRRK2 gene in Parkinson disease yields new mutations. Neurology. 2005;65(5):741-4.
671 11. Hatano T, Funayama M, Kubo SI, Mata IF, Oji Y, Mori A, et al. Identification of a Japanese
672 family with LRRK2 p.R1441G-related Parkinson's disease. Neurobiol Aging. 2014;35(11):2656.e17-.e23.
673 12. Takanashi M, Funayama M, Matsuura E, Yoshino H, Li Y, Tsuyama S, et al. Isolated nigral
674 degeneration without pathological protein aggregation in autopsied brains with LRRK2 p.R1441H
675 homozygous and heterozygous mutations. Acta Neuropathol Commun. 2018;6(1):105.
676 13. Nichols WC, Pankratz N, Hernandez D, Paisan-Ruiz C, Jain S, Halter CA, et al. Genetic
677 screening for a single common LRRK2 mutation in familial Parkinson's disease. Lancet.
678 2005;365(9457):410-2.
679 14. Di Fonzo A, Rohé CF, Ferreira J, Chien HF, Vacca L, Stocchi F, et al. A frequent LRRK2 gene
680 mutation associated with autosomal dominant Parkinson's disease. Lancet. 2005;365(9457):412-5.
681 15. Hernandez DG, Paisan-Ruiz C, McInerney-Leo A, Jain S, Meyer-Lindenberg A, Evans EW, et al.
682 Clinical and positron emission tomography of Parkinson's disease caused by LRRK2. Ann Neurol.
683 2005;57(3):453-6.

684 16. Kachergus J, Mata IF, Hulihan M, Taylor JP, Lincoln S, Aasly J, et al. Identification of a novel
685 LRRK2 mutation linked to autosomal dominant parkinsonism: evidence of a common founder across
686 European populations. Am J Hum Genet. 2005;76(4):672-80.
687 17. Bosgraaf L, Van Haastert PJ. Roc, a Ras/GTPase domain in complex proteins. Biochim Biophys
688 Acta. 2003;1643(1-3):5-10.
689 18. Marin I. The Parkinson disease gene LRRK2: evolutionary and structural insights. Mol Biol Evol.
690 2006;23(12):2423-33.
691 19. Marín I. Ancient origin of the Parkinson disease gene LRRK2. J Mol Evol. 2008;67(1):41-50.
692 20. Biskup S, Moore DJ, Rea A, Lorenz-Deperieux B, Coombes CE, Dawson VL, et al. Dynamic and
693 redundant regulation of LRRK2 and LRRK1 expression. BMC Neurosci. 2007;8:102.
694 21. Schulte EC, Ellwanger DC, Dihanich S, Manzoni C, Stangl K, Schormair B, et al. Rare variants
695 in LRRK1 and Parkinson's disease. Neurogenetics. 2014;15(1):49-57.
696 22. Deng J, Lewis PA, Greggio E, Sluch E, Beilina A, Cookson MR. Structure of the ROC domain
697 from the Parkinson's disease-associated leucine-rich repeat kinase 2 reveals a dimeric GTPase. Proc Natl
698 Acad Sci U S A. 2008;105(5):1499-504.
699 23. Mills RD, Liang LY, Lio DS, Mok YF, Mulhern TD, Cao G, et al. The Roc-COR tandem domain
700 of leucine-rich repeat kinase 2 forms dimers and exhibits conventional Ras-like GTPase properties. J
701 Neurochem. 2018;147(3):409-28.
702 24. Myasnikov A, Zhu H, Hixson P, Xie B, Yu K, Pitre A, et al. Structural analysis of the full-length
703 human LRRK2. Cell. 2021;184(13):3519-27 e10.
704 25. Tong Y, Yamaguchi H, Giaime E, Boyle S, Kopan R, Kelleher RJ, 3rd, et al. Loss of leucine-rich
705 repeat kinase 2 causes impairment of protein degradation pathways, accumulation of alpha-synuclein, and
706 apoptotic cell death in aged mice. Proc Natl Acad Sci U S A. 2010;107(21):9879-84.
707 26. Tong Y, Giaime E, Yamaguchi H, Ichimura T, Liu Y, Si H, et al. Loss of leucine-rich repeat kinase
708 2 causes age-dependent bi-phasic alterations of the autophagy pathway. Mol Neurodegener. 2012;7:2.
709 27. Herzig MC, Kolly C, Persohn E, Theil D, Schweizer T, Hafner T, et al. LRRK2 protein levels are
710 determined by kinase function and are crucial for kidney and lung homeostasis in mice. Hum Mol Genet.
711 2011;20(21):4209-23.
712 28. Tian Y, Lv J, Su Z, Wu T, Li X, Hu X, et al. LRRK2 plays essential roles in maintaining lung
713 homeostasis and preventing the development of pulmonary fibrosis. Proc Natl Acad Sci U S A.
714 2021;118(35).
715 29. Tong Y, Shen J. Genetic analysis of Parkinson's disease-linked leucine-rich repeat kinase 2.
716 Biochem Soc Trans. 2012;40(5):1042-6.
717 30. Giaime E, Tong Y, Wagner LK, Yuan Y, Huang G, Shen J. Age-Dependent Dopaminergic

718 Neurodegeneration and Impairment of the Autophagy-Lysosomal Pathway in LRRK Deficient Mice.
719 Neuron. 2017;96(4):796-807.e6.
720 31. Huang G, Bloodgood DW, Kang J, Shahapal A, Chen P, Kaganovsky K, et al. Motor Impairments
721 and Dopaminergic Defects Caused by Loss of Leucine-Rich Repeat Kinase Function in Mice. J Neurosci.
722 2022;42(23):4755-65.
723 32. Backman CM, Malik N, Zhang Y, Shan L, Grinberg A, Hoffer BJ, et al. Characterization of a
724 mouse strain expressing Cre recombinase from the 3' untranslated region of the dopamine transporter
725 locus. Genesis. 2006;44(8):383-90.
726 33. Rodriguez CI, Buchholz F, Galloway J, Sequerra R, Kasper J, Ayala R, et al. High-efficiency
727 deleter mice show that FLPe is an alternative to Cre-loxP. Nat Genet. 2000;25(2):139-40.
728 34. Schwenk F, Baron U, Rajewsky K. A cre-transgenic mouse strain for the ubiquitous deletion of
729 loxP-flanked gene segments including deletion in germ cells. Nucleic Acids Res. 1995;23(24):5080-1.
730 35. Madisen L, Zwingman TA, Sunkin SM, Oh SW, Zariwala HA, Gu H, et al. A robust and high-
731 throughput Cre reporting and characterization system for the whole mouse brain. Nat Neurosci.
732 2010;13(1):133-40.
733 36. Healy DG, Falchi M, O'Sullivan SS, Bonifati V, Durr A, Bressman S, et al. Phenotype, genotype,
734 and worldwide genetic penetrance of LRRK2-associated Parkinson's disease: a case-control study. Lancet
735 Neurol. 2008;7(7):583-90.
736 37. Tong Y, Pisani A, Martella G, Karouani M, Yamaguchi H, Pothos EN, et al. R1441C mutation in
737 LRRK2 impairs dopaminergic neurotransmission in mice. Proc Natl Acad Sci U S A.
738 2009;106(34):14622-7.
739 38. Yue M, Hinkle KM, Davies P, Trushina E, Fiesel FC, Christenson TA, et al. Progressive
740 dopaminergic alterations and mitochondrial abnormalities in LRRK2 G2019S knock-in mice. Neurobiol
741 Dis. 2015;78:172-95.
742 39. Xing W, Liu J, Cheng S, Vogel P, Mohan S, Brommage R. Targeted disruption of leucine-rich
743 repeat kinase 1 but not leucine-rich repeat kinase 2 in mice causes severe osteopetrosis. J Bone Miner
744 Res. 2013;28(9):1962-74.
745 40. Guo L, Girisha KM, Iida A, Hebbar M, Shukla A, Shah H, et al. Identification of a novel LRRK1
746 mutation in a family with osteosclerotic metaphyseal dysplasia. J Hum Genet. 2017;62(3):437-41.
747 41. Sheng Z, Zhang S, Bustos D, Kleinheinz T, Le Pichon CE, Dominguez SL, et al. Ser1292
748 autophosphorylation is an indicator of LRRK2 kinase activity and contributes to the cellular effects of PD
749 mutations. Science translational medicine. 2012;4(164):164ra1.
750 42. Gloeckner CJ, Boldt K, von Zweydorf F, Helm S, Wiesent L, Sarioglu H, et al. Phosphopeptide
751 analysis reveals two discrete clusters of phosphorylation in the N-terminus and the Roc domain of the

752 Parkinson-disease associated protein kinase LRRK2. J Proteome Res. 2010;9(4):1738-45.
753 43. Marchand A, Drouyer M, Sarchione A, Chartier-Harlin MC, Taymans JM. LRRK2
754 Phosphorylation, More Than an Epiphenomenon. Front Neurosci. 2020;14:527.
755 44. Steger M, Tonelli F, Ito G, Davies P, Trost M, Vetter M, et al. Phosphoproteomics reveals that
756 Parkinson's disease kinase LRRK2 regulates a subset of Rab GTPases. eLife. 2016;5:e12813.
757 45. Li Y, Liu W, Oo TF, Wang L, Tang Y, Jackson-Lewis V, et al. Mutant LRRK2(R1441G) BAC
758 transgenic mice recapitulate cardinal features of Parkinson's disease. Nat Neurosci. 2009;12(7):826-8.
759 46. Lin X, Parisiadou L, Gu XL, Wang L, Shim H, Sun L, et al. Leucine-rich repeat kinase 2
760 regulates the progression of neuropathology induced by Parkinson's-disease-related mutant alpha-
761 synuclein. Neuron. 2009;64(6):807-27.
762 47. Li X, Patel JC, Wang J, Avshalumov MV, Nicholson C, Buxbaum JD, et al. Enhanced striatal
763 dopamine transmission and motor performance with LRRK2 overexpression in mice is eliminated by
764 familial Parkinson's disease mutation G2019S. J Neurosci. 2010;30(5):1788-97.
765 48. Melrose HL, Dachsel JC, Behrouz B, Lincoln SJ, Yue M, Hinkle KM, et al. Impaired
766 dopaminergic neurotransmission and microtubule-associated protein tau alterations in human LRRK2
767 transgenic mice. Neurobiol Dis. 2010;40(3):503-17.
768 49. Daher JP, Pletnikova O, Biskup S, Musso A, Gellhaar S, Galter D, et al. Neurodegenerative
769 phenotypes in an A53T α-synuclein transgenic mouse model are independent of LRRK2. Hum Mol
770 Genet. 2012;21(11):2420-31.
771 50. Tsika E, Kannan M, Foo CS, Dikeman D, Glauser L, Gellhaar S, et al. Conditional expression of
772 Parkinson's disease-related R1441C LRRK2 in midbrain dopaminergic neurons of mice causes nuclear
773 abnormalities without neurodegeneration. Neurobiol Dis. 2014;71:345-58.
774 51. Liu G, Sgobio C, Gu X, Sun L, Lin X, Yu J, et al. Selective expression of Parkinson's disease-
775 related Leucine-rich repeat kinase 2 G2019S missense mutation in midbrain dopaminergic neurons
776 impairs dopamine release and dopaminergic gene expression. Hum Mol Genet. 2015;24(18):5299-312.
777 52. Mikhail F, Calingasan N, Parolari L, Subramanian A, Yang L, Flint Beal M. Lack of exacerbation
778 of neurodegeneration in a double transgenic mouse model of mutant LRRK2 and tau. Hum Mol Genet.
779 2015;24(12):3545-56.
780 53. Xiong Y, Neifert S, Karuppagounder SS, Stankowski JN, Lee BD, Grima JC, et al.
781 Overexpression of Parkinson's Disease-Associated Mutation LRRK2 G2019S in Mouse Forebrain
782 Induces Behavioral Deficits and α-Synuclein Pathology. eNeuro. 2017;4(2).
783 54. Ramonet D, Daher JP, Lin BM, Stafa K, Kim J, Banerjee R, et al. Dopaminergic neuronal loss,
784 reduced neurite complexity and autophagic abnormalities in transgenic mice expressing G2019S mutant
785 LRRK2. PloS one. 2011;6(4):e18568.

786 55. Xiong Y, Neifert S, Karuppagounder SS, Liu Q, Stankowski JN, Lee BD, et al. Robust kinase-
787 and age-dependent dopaminergic and norepinephrine neurodegeneration in LRRK2 G2019S transgenic
788 mice. Proc Natl Acad Sci U S A. 2018;115(7):1635-40.
789 56. Zhang P, Fan Y, Ru H, Wang L, Magupalli VG, Taylor SS, et al. Crystal structure of the WD40
790 domain dimer of LRRK2. Proc Natl Acad Sci U S A. 2019;116(5):1579-84.
791 57. Greggio E, Zambrano I, Kaganovich A, Beilina A, Taymans JM, Daniels V, et al. The Parkinson
792 disease-associated leucine-rich repeat kinase 2 (LRRK2) is a dimer that undergoes intramolecular
793 autophosphorylation. J Biol Chem. 2008;283(24):16906-14.
794 58. Sen S, Webber PJ, West AB. Dependence of leucine-rich repeat kinase 2 (LRRK2) kinase activity
795 on dimerization. J Biol Chem. 2009;284(52):36346-56.
796 59. Jorgensen ND, Peng Y, Ho CC, Rideout HJ, Petrey D, Liu P, et al. The WD40 domain is required
797 for LRRK2 neurotoxicity. PloS one. 2009;4(12):e8463.
798 60. Dachsel JC, Nishioka K, Vilariño-Güell C, Lincoln SJ, Soto-Ortolaza AI, Kachergus J, et al.
799 Heterodimerization of Lrrk1-Lrrk2: Implications for LRRK2-associated Parkinson disease. Mech Ageing
800 Dev. 2010;131(3):210-4.
801 61. Farrer MJ, Stone JT, Lin CH, Dächsel JC, Hulihan MM, Haugarvoll K, et al. Lrrk2 G2385R is an
802 ancestral risk factor for Parkinson's disease in Asia. Parkinsonism Relat Disord. 2007;13(2):89-92.
803 62. Kim JM, Lee JY, Kim HJ, Kim JS, Shin ES, Cho JH, et al. The LRRK2 G2385R variant is a risk
804 factor for sporadic Parkinson's disease in the Korean population. Parkinsonism Relat Disord.
805 2010;16(2):85-8.
806 63. An XK, Peng R, Li T, Burgunder JM, Wu Y, Chen WJ, et al. LRRK2 Gly2385Arg variant is a risk
807 factor of Parkinson's disease among Han-Chinese from mainland China. Eur J Neurol. 2008;15(3):301-5.
808 64. Xie CL, Pan JL, Wang WW, Zhang Y, Zhang SF, Gan J, et al. The association between the
809 LRRK2 G2385R variant and the risk of Parkinson's disease: a meta-analysis based on 23 case-control
810 studies. Neurol Sci. 2014;35(10):1495-504.
811 65. Rudenko IN, Kaganovich A, Hauser DN, Beylina A, Chia R, Ding J, et al. The G2385R variant of
812 leucine-rich repeat kinase 2 associated with Parkinson's disease is a partial loss-of-function mutation. The
813 Biochemical journal. 2012;446(1):99-111.
814 66. Carrion MDP, Marsicano S, Daniele F, Marte A, Pischedda F, Di Cairano E, et al. The LRRK2
815 G2385R variant is a partial loss-of-function mutation that affects synaptic vesicle trafficking through
816 altered protein interactions. Sci Rep. 2017;7(1):5377.
817 67. Kang J, Watanabe H, Shen J. Protocols for assessing neurodegenerative phenotypes in
818 Alzheimer’s mouse models. STAR Protocols. 2021;2(3).
819 68. Yu H, Kessler J, Shen J. Heterogeneous populations of ES cells in the generation of a floxed

820 Presenilin-1 allele. Genesis. 2000;26(1):5-8.
821 69. Yamaguchi H, Shen J. Histological analysis of neurodegeneration in the mouse brain. Methods
822 Mol Biol. 2013;1004:91-113.
823 70. Nelson EL, Liang CL, Sinton CM, German DC. Midbrain dopaminergic neurons in the mouse:
824 computer-assisted mapping. J Comp Neurol. 1996;369(3):361-71.
825 71. Huang G, Bloodgood DW, Kang J, Shahapal A, Chen P, Kaganovsky K, et al. Motor impairments
826 and dopamingergic defects caused by loss of LRRK function in mice. J Neurosci. 2022;42(23):4755-65.
827 72. Walton WH. Feret‘s Statistical Diameter as a Measure of Particle Size. Nature.
828 1948;162(4113):329-30.

829

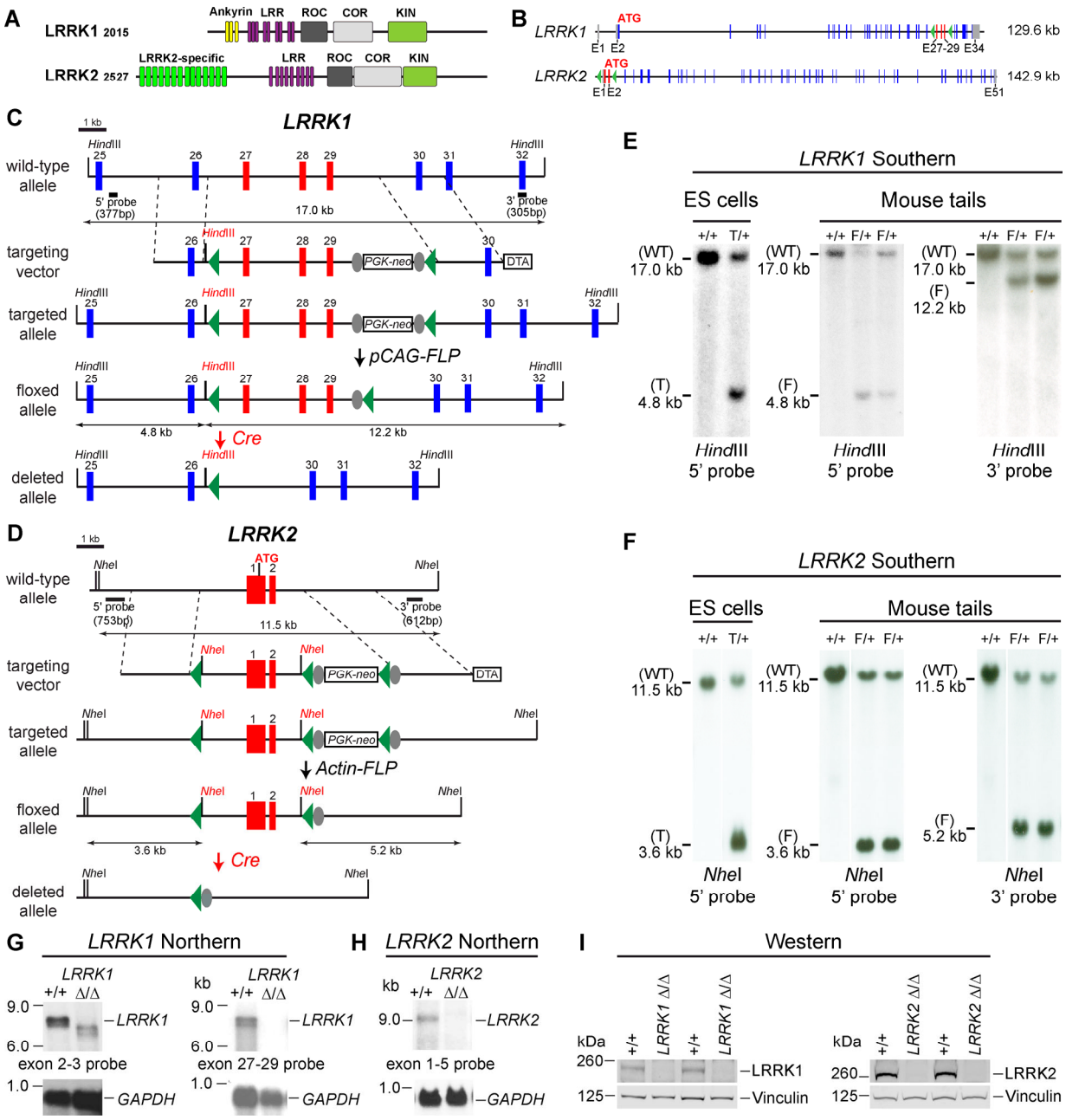

Figure 1. Generation and characterization of floxed and deleted *LRRK1* and *LRRK2* alleles

(**A**) Schematic illustrations of human LRRK1 and LRRK2 proteins showing similar functional domains. $LRRK1_{2015}$ protein is derived from exons 2-34 (Ensembl Genome Database: ENSG00000154237). $LRRK2_{2527}$ protein is derived from exons 1-51 (ENSG00000188906). LRR: Leucine rich repeats; Roc: Ras-of-complex; COR: C-terminal of Roc; KIN: Kinase domain.

(**B**) Schematic illustrations of the gene structures of mouse *LRRK1* and *LRRK2*. The boxes in blue are exons that encode the LRRK1 and LRRK2 proteins, and the gray boxes represent the 5' and 3' UTRs. The exons are not drawn in scale. The start codon ATG is in exon 2 of *LRRK1* and exon 1 of *LRRK2*. The exons 27-29 of *LRRK1* and the promoter/exons 1-2 of *LRRK2* are flanked with *loxP* sites (green arrowheads).

841 (**C**) Targeting strategy for the generation of the targeted, floxed, and deleted *LRRK1* alleles. The red
842 boxes represent the targeted exons 27-29, and the blue boxes represent the untargeted exons. The
843 locations and sizes of the 5' and 3' external probes are shown. The targeting vector contains the 5' and 3'
844 homologous regions (marked by dashed lines) and the middle-targeted region, which includes a *loxP* site
845 (green arrowhead) in intron 26 (1,288 bp upstream of exon 27) and the *PGK-neo* selection cassette
846 flanked by two *FRT* (FLP recognition target) sequences (gray circles) followed by another *loxP* site in
847 intron 29 (1,023 bp downstream of exon 29). A negative selection cassette encoding diphtheria toxin
848 fragment A (DTA) is also included in the targeting vector to reduce ES cells bearing randomly inserted
849 targeting vectors. ES cells carrying the correctly targeted *LRRK1* allele were transfected with *pCAG-FLP*
850 to remove the *PGK-neo* cassette and generate the floxed *LRRK1* allele. Floxed *LRRK1* mice were bred
851 with *CMV-Cre* transgenic mice to generate germline deleted *LRRK1* mice. Detailed strategy for
852 generating targeting vector and DNA sequence of floxed *LRRK1* allele can be found in Figure 1-figure
853 supplement 1 and 2, respectively.

854 (**D**) Southern analysis of the targeted and floxed *LRRK1* alleles. Genomic DNA from ES cells or mouse
855 tails was digested with *Hind*III and hybridized with the 5' or 3' external probe. For the 5' probe, the
856 resulting 17.0 kb and 4.8 kb bands represent the wild-type (WT) and the targeted (T) or floxed (F) alleles,
857 respectively. For the 3' probe, the resulting 17.0 kb and 12.2 kb bands represent the WT and the floxed (F)
858 alleles, respectively. Detailed Southern strategy can be found in Figure 1-figure supplement 3.

859 **(E**) Targeting strategy for the generation of the targeted, floxed, and deleted *LRRK2* alleles. The red
860 boxes represent *LRRK2* exons 1 and 2, and the start codon ATG resides in exon 1. The locations and sizes
861 of the 5' and 3' external probes are shown. The targeting vector contains the 5' and 3' homologous regions
862 (marked by dashed lines) and the middle targeted region (from the promoter region to intron 2), which
863 includes a *loxP* site (green arrowhead) upstream (1,768 bp) of the transcription initiation site and the
864 *PGK-neo* selection cassette flanked by two *FRT* sequences (gray circles) and two *loxP* sites (green
865 arrowheads) in intron 2 (878 bp downstream of exon 2). A negative selection cassette encoding DTA is
866 also included in the targeting vector. Mice carrying the correctly targeted *LRRK2* allele were crossed with
867 *Actin-FLP* deleter mice to generate floxed *LRRK2* mice, which were bred with *CMV-Cre* transgenic mice
868 to generate germline deleted *LRRK2* mice. Detailed strategy for generating targeting vector and DNA
869 sequence of floxed *LRRK2* allele can be found in Figure 1-figure supplement 4 and 5, respectively.

870 (**F**) Southern analysis of the targeted and floxed *LRRK2* alleles. Genomic DNA from ES cells or mouse
871 tails was digested with *Nhe*I and hybridized with the 5' or 3' external probe. For the 5' probe, the resulting
872 11.5 kb and 3.6 kb bands represent the wild-type (WT) and the targeted (T) or floxed (F) alleles,
873 respectively. For the 3' probe, the resulting 11.5 kb and 5.2 kb bands represent the WT and the floxed (F)
874 alleles, respectively. Detailed Southern strategy can be found in Figure 1-figure supplement 6.

875 (**G**) Northern analysis of poly(A)+ RNA prepared from the lung of mice carrying homozygous germline
876 deleted (Δ/Δ) *LRRK1* alleles derived from the floxed *LRRK1* alleles using the cDNA probe of exons 2-3
877 (*left*) and exons 27-29 (*right*). Using the upstream exons 2-3 probe, the *LRRK1* transcripts in wild-type
878 mice are the expected size of ~7.4 kb, whereas the detected *LRRK1* transcripts in *LRRK1* Δ/Δ mice are
879 truncated, consistent with the deletion of exons 27-29 (625 bp), which results in a frameshift and likely
880 degradation of the truncated *LRRK1* mRNA. Using a probe specific for exons 27-29, there is no *LRRK1*
881 transcript in *LRRK1* Δ/Δ mice, as expected. Both blots were hybridized with a *GAPDH* probe as loading
882 controls. Detailed Northern strategy and full-size blots are included in Figure 1-figure supplement 7 and 8,
883 respectively. See also Figure 1-figure supplement 9.

884 (**H**) Northern analysis of total RNA prepared from the neocortex of mice carrying homozygous germline
885 *LRRK2* deleted (Δ/Δ) alleles using the cDNA probe of exons 1-5 shows the absence of *LRRK2* transcripts.
886 The blot was hybridized with a *GAPDH* probe as a loading control. The full-size blot is included in
887 Figure 1-figure supplement 10. See also Figure 1-figure supplement 11

888 (**I**) *Left*: Western analysis of wild-type (+/+) and homozygous *LRRK1* Δ/Δ brains show the absence of
889 LRRK1 protein. *Right*: Western analysis of the neocortex of wild-type (+/+) and homozygous *LRRK2* Δ/Δ
890 mice shows the absence of LRRK2 protein. Vinculin was used as a loading control. Full-size blots are
891 included in Figure 1-Source Data 1.

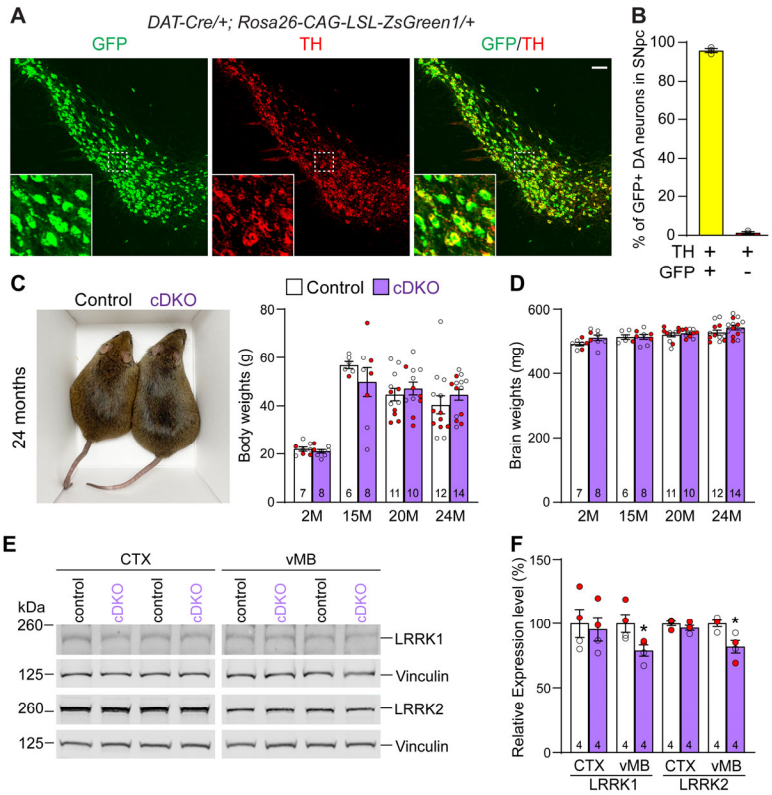

Figure 2. Generation and characterization of DA neuron-specific *LRRK* cDKO mice

(**A**) Immunostaining of GFP and/or TH in the SNpc of *DAT-Cre/+; Rosa26-CAG-LSL-ZsGreen1/+* mice at 2 months of age. Cre recombinase is expressed under the control of the *DAT* endogenous promoter and removes the floxed "stop" cassette, resulting in the expression of EGFP under the control of the ubiquitous *CAG* promoter.

(**B**) Quantification of GFP+/TH+ and TH+ cells shows that 99% of TH+ DA neurons (722 ± 46 TH+ cells per brain) in the SNpc are also GFP+ (713 ± 46 cells per brain), indicating that *DAT-Cre* mediated recombination occurs in essentially all TH+ DA neurons. N = 3 mice, 3 comparable sections per hemisphere, 320 µm apart. Raw quantification data are included in Figure 2-Source Data 1.

(**C**) Similar body weight between *LRRK* cDKO mice and littermate controls at all ages examined ($F_{1,73}$ = 0.0210, p = 0.8853; 2M, 20M, 25M: p > 0.9999; 15M: p = 0.7468, two-way ANOVA with Bonferroni's post hoc multiple comparisons). Raw quantification data are included in Figure 2-Source Data 2.

(**D**) Similar brain weight between *LRRK* cDKO and control mice ($F_{1,61}$ = 0.0440, p = 0.8345; 2M: p = 0.3893; 15M: p > 0.9999; 20M: p > 0.9999; 25M: p = 0.3223, two-way ANOVA with Bonferroni's post hoc multiple comparisons). Raw quantification data are included in Figure 2-Source Data 2.

(**E**) Western analysis of LRRK1 and LRRK2 proteins in the dissected cerebral cortex (CTX) and ventral midbrain (vMB) of *LRRK* cDKO and littermate controls at 2 months of age. Full-size blots are included in Figure 2-Source Data 3.

(**F**) Quantification shows significant decreases of LRRK1 and LRRK2 in the dissected ventral midbrain of *LRRK* cDKO mice (LRRK1, p = 0.0432; LRRK2, p = 0.0162, unpaired two-tailed Student's *t*-test), compared to controls, but not in the dissected cortex of cDKO mice (LRRK1, p = 0.7648; LRRK2, p = 0.2325). Raw quantification data are included in Figure 2-Source Data 4.

The number in the column indicates the number of mice used in the study. Red-filled and open circles represent data obtained from individual male and female mice, respectively. All data are expressed as mean ± SEM. *p < 0.05. Scale bar: 100 µm.

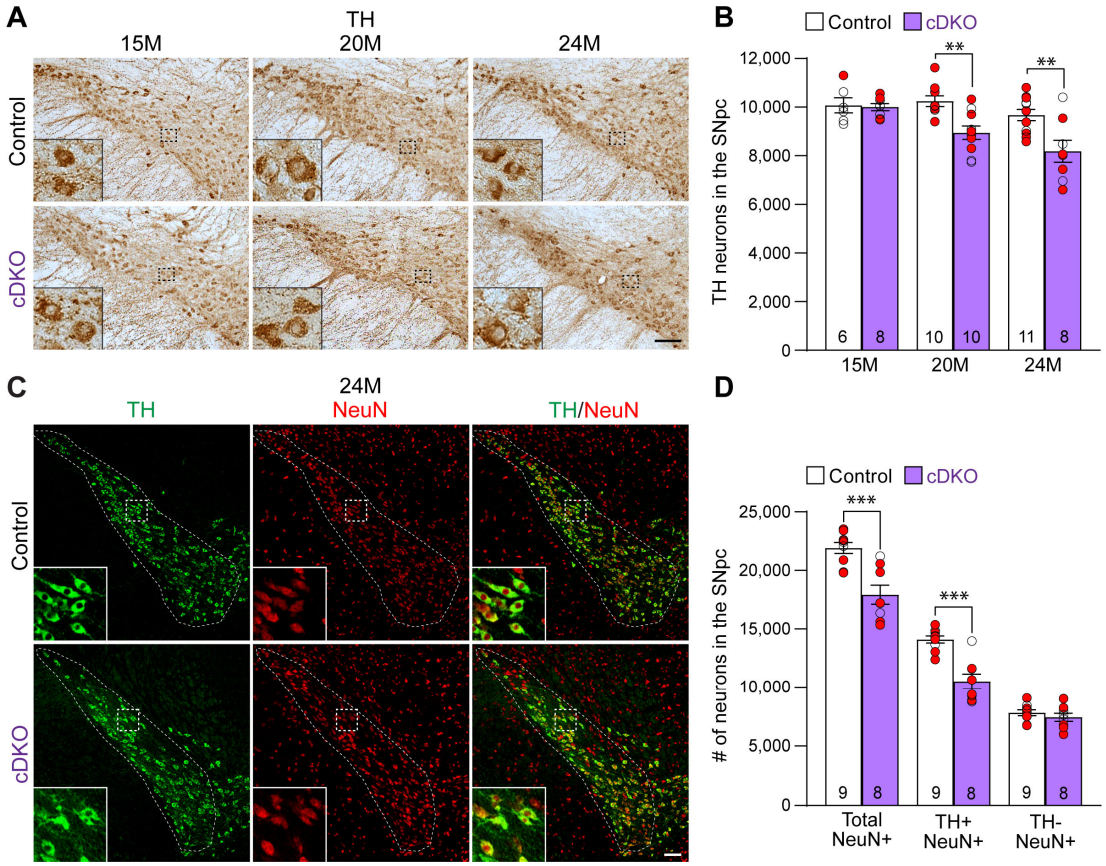

Figure 3. Age-dependent loss of DA neurons in the SNpc of *LRRK* cDKO mice

(**A**) TH immunostaining shows TH+ DA neurons in the SNpc of *LRRK* cDKO and littermate controls at the age of 15, 20, and 24 months. Higher power views of the boxed areas show grossly normal DA neuron morphology in *LRRK* cDKO mice.

(**B**) Quantification of all TH+ DA neurons in the SNpc reveals similar numbers of DA neurons in *LRRK* cDKO mice (10,000 ± 141) and littermate controls (10,077 ± 310, $p > 0.9999$) at 15 months of age. At 20 months of age, the number of DA neurons in the SNpc of *LRRK* cDKO mice (8,948 ± 273) is significantly reduced, compared to control mice (10,244 ± 220, $F_{1,46} = 16.59$, $p = 0.0002$; $p = 0.0041$, two-way ANOVA with Bonferroni's post hoc multiple comparisons). By 24 months of age, the reduction of DA neurons in the SNpc of *LRRK* cDKO mice (8,188 ± 452) relative to controls (9,675 ± 232, $p = 0.0010$) is greater, compared to that at 20 months of age. Raw quantification data are included in Figure 3-Source Data 1.

(**C**) Immunohistological analysis of TH and NeuN shows TH+ dopaminergic neurons (green) and NeuN+ neurons (red) in the SNpc of *LRRK* cDKO mice and controls at 24 months of age.

(**D**) Quantification of NeuN+ cells in the SNpc shows that the number of NeuN+ neurons in *LRRK* cDKO mice (17,923 ± 813) is significantly lower than that in control mice (21,907 ± 469, $p = 0.0006$, Student's *t*-test), indicating loss of neurons in the SNpc of *LRRK* cDKO mice. All TH+ cells are NeuN+. The number of TH+/NeuN+ cells in the SNpc of *LRRK* cDKO mice (10,500 ± 644) is also lower, compared to control mice (14,102 ± 310, $p = 0.0001$). There is no significant difference in the number of NeuN+/TH- neurons between littermate controls (7,804 ± 249) and cDKO mice (7,423 ± 344, $p = 0.3747$). Raw quantification data are included in Figure 3-Source Data 2.

The number in the column indicates the number of mice used in the study. Red-filled and open circles represent data obtained from individual male and female mice, respectively. All data are expressed as mean ± SEM. $^{**}p < 0.01$, $^{***}p < 0.001$. Scale bar: 100 μm.

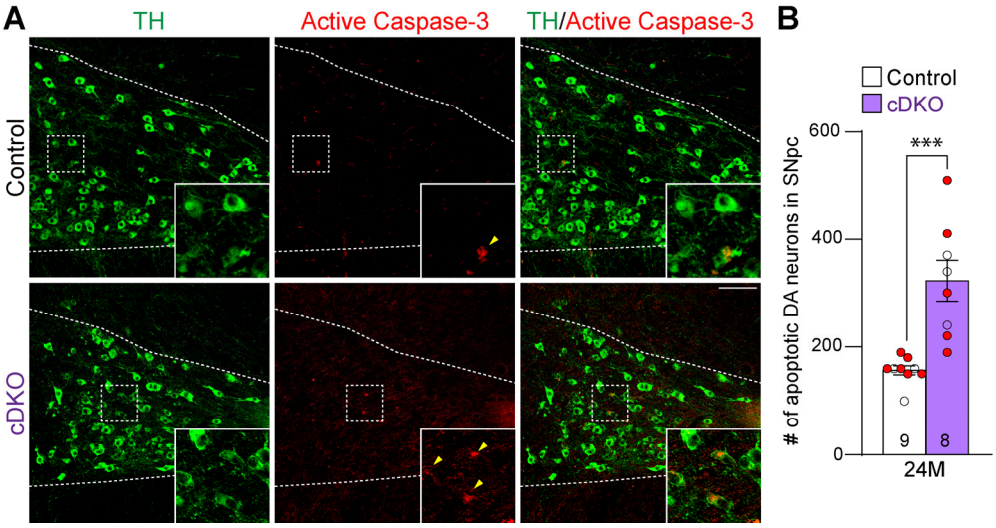

Figure 4. Increases in apoptotic DA neurons in the SNpc of *LRRK* cDKO mice

(**A**) Representative images of TH and active Caspase-3 immunostaining show TH+ DA neurons (green) and active Caspase-3+ apoptotic cells (red) in the SNpc of *LRRK* cDKO and control mice at the age of 24 months.

(**B**) Quantification of active Caspase-3+/TH+ cells shows significant increases of apoptotic DA neurons in the SNpc of *LRRK* cDKO mice (323 ± 38) at 24 months of age, relative to controls (157 ± 8, $p = 0.0004$, unpaired Student's *t*-test). Raw quantification data are included in Figure 4-Source Data 1.

The number in the column indicates the number of mice used in the study. Red-filled and open circles represent data obtained from individual male and female mice, respectively. All data are expressed as mean ± SEM. ***$p < 0.001$. Scale bar: 100 μm.

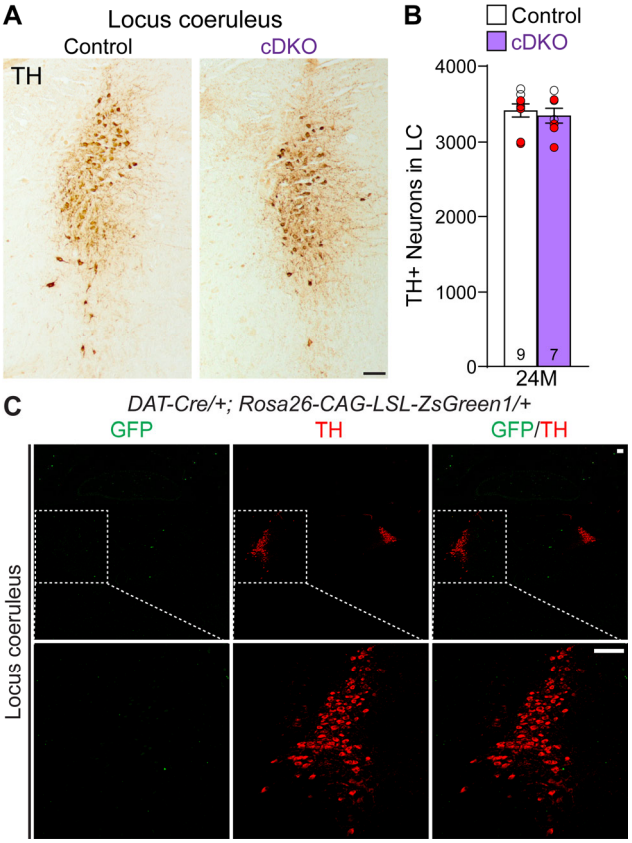

Figure 5. Normal number of TH+ noradrenergic neurons in the LC of *LRRK* cDKO mice

(**A**) Representative images of TH+ noradrenergic neurons in the locus coeruleus (LC) of *LRRK* cDKO mice and littermate controls at 24 months of age.

(**B**) Quantification of TH+ neurons shows similar numbers of TH+ noradrenergic neurons in the LC of *LRRK* cDKO mice (3,350 ± 99) and controls (3,419 ± 86, p = 0.6057, unpaired Student's *t*-test). Raw quantification data are included in Figure 5-Source Data 1.

(**C**) *Top*: Immunostaining of TH and GFP in the LC of *DAT-Cre/+; Rosa26-CAG-LSL-ZsGreen1/+* mice at 2 months of age. There is no GFP+ (green) cell in the LC, indicating that *DAT-Cre* is not expressed in the LC. *Bottom*: Higher power views of the boxed areas.

The number in the column indicates the number of mice used in the study. Red-filled and open circles represent data obtained from individual male and female mice, respectively. All data are expressed as mean ± SEM. Scale bar: 100 μm.

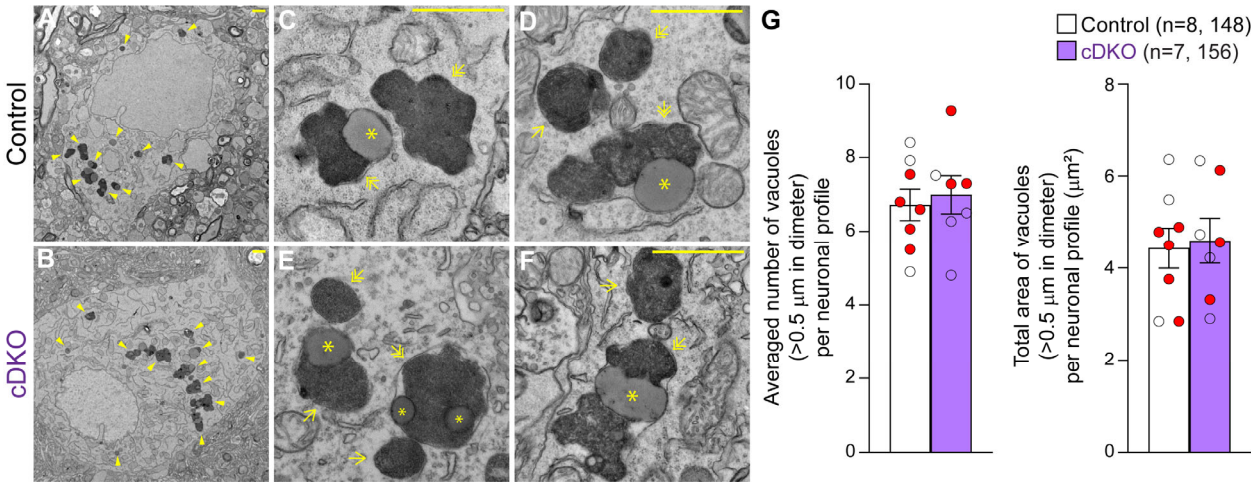

Figure 6. Unchanged number of electron-dense vacuoles in the SNpc of *LRRK* cDKO mice

(**A**, **B**) Representative EM images showing electron-dense vacuoles (arrowheads) in SNpc neurons of cDKO mice and littermate controls at the age of 25 months.

(**C-F**) Higher power views showing various electron-dense vacuoles, autolysosomes (single arrows), autophagosomes (double arrows), and lipid-containing vacuoles (asterisks) in SNpc neurons of littermate control (**C**, **D**) and cDKO (**E**, **F**) mice.

(**G**) *Left*: The average number of electron-dense vacuoles (>0.5 μm in diameter) in the SNpc neuronal profiles per mouse is not significantly different between *LRRK* cDKO mice and littermate controls at the age of 25 months (Control: 6.72 ± 0.43; cDKO: 6.99 ± 0.52, p = 0.6839, unpaired two-tailed Student's *t*-test). Right: The total area of electron-dense vacuoles (>0.5 μm in diameter) in the SNpc neuronal profiles per mouse is similar between *LRRK* cDKO and littermate controls (Control: 4.43 ± 0.44 μm^2; cDKO: 4.60 ± 0.49 μm^2, p = 0.8048). Raw quantification data are included in Figure 6-Source Data 1.

The value in parentheses indicates the number of mice (left) and neuron profiles (right) used in the quantification. Red-filled and open circles represent data obtained from individual male and female mice, respectively. All data are expressed as mean ± SEM. Scale bar: 1 μm.

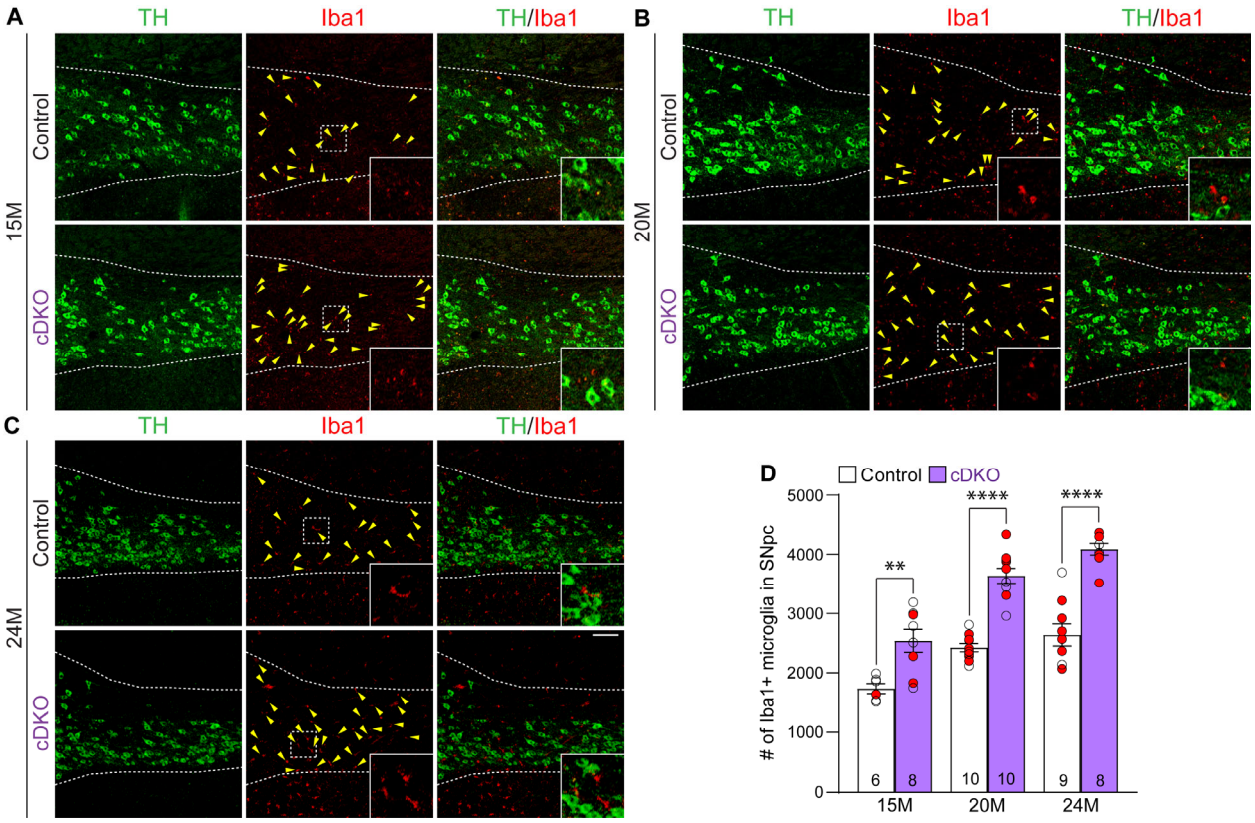

983

984 **Figure 7. Elevated microgliosis in the SNpc of *LRRK* cDKO mice**

985 (**A-C**) Representative images of Iba1+ microglia (red, marked by yellow arrowheads) and TH+
986 dopaminergic neurons (green) in the SNpc of *LRRK* DKO mice and controls at 15 (A), 20 (B), and 24 (C)
987 months of age.

988 (**D**) Quantification of Iba1+ microglia shows significant increases in the number of Iba1+ microglia in the
989 SNpc of *LRRK* cDKO mice compared to control mice at 15 (control: 1736.7 ± 82.9, cDKO: 2541.3 ±
990 193.0, $p = 0.0017$, two-way ANOVA with Bonferroni's post hoc multiple comparisons), 20 (control:
991 2426.0 ± 67.7, cDKO: 3639.0 ± 127.1, $p < 0.0001$), and 24 months of age (control: 2640.0 ± 187.1,
992 cDKO: 4088.8 ± 100.3, $p < 0.0001$). Raw quantification data are included in Figure 7-Source Data 1.

993 The number in the column indicates the number of mice used in the study. Red-filled and open circles
994 represent data obtained from individual male and female mice, respectively. All data are expressed as
995 mean ± SEM. ****$p < 0.0001$. Scale bar: 100 μm.

Figure 1-figure supplement 1. Generation of the *LRRK1* targeting vector

1) The *left middle* arm was amplified by PCR from mouse BAC DNA (Clone #: RP23-213J23, BACPAC Resources Center) using primers P3 and P4. The resulting PCR product (2,079 bp) containing part of *LRRK1* intron 26, exon 27, and part of intron 27 was subcloned into the pGEM-T Vector (Promega, Cat#; A1360) by TA ligation to generate pLRRK1#1 (pLM1).

P3: 5'CCAGTCACTTCTCCACCTCAGGGAAAATGG (30 bp)

P4: 5'CCTTGT*GGTACC*CGGACCTTCTATCACCTTTATCC (35 bp): *Kpn*I (*GGTACC*) is an endogenous restriction site.

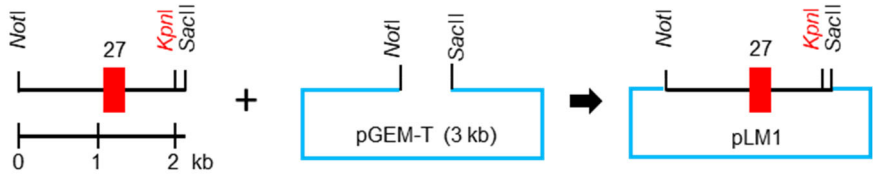

2) The *right middle* arm was amplified from mouse BAC DNA (Clone #: RP23-213J23) using primers P5 and P6. The resulting PCR product (3,403 bp) containing part of *LRRK1* intron 27, exon 28, intron 28, exon 29, and part of intron 29 was subcloned into the pGEM-T Vector by TA ligation to generate pLRRK1#2 (pLM2).

P5: 5'GGTCCG*GGTACC*ACAAGGTGCTGGTTAAGTGCC (33 bp): *Kpn*I (*GGTACC*) is an endogenous restriction site.

P6: 5'AGCAGACCTCTTGCCTTCTACTACTGACTG (30 bp)

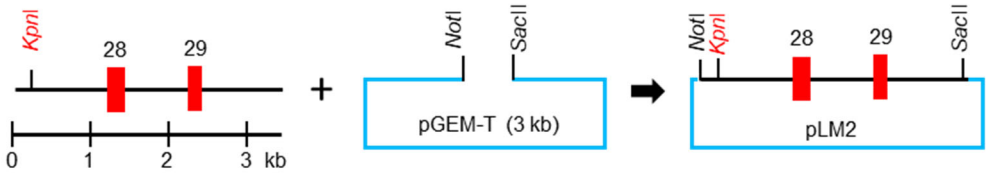

3) pLRRK1#1 (pLM1) was digested with *Not*I and *Kpn*I, then subcloned into the *Not*I and *Kpn*I sites of pLRRK1#2 (pLM2) to generate the pLRRK1#3 (pLM3) plasmid which contains the *middle* homologous region.

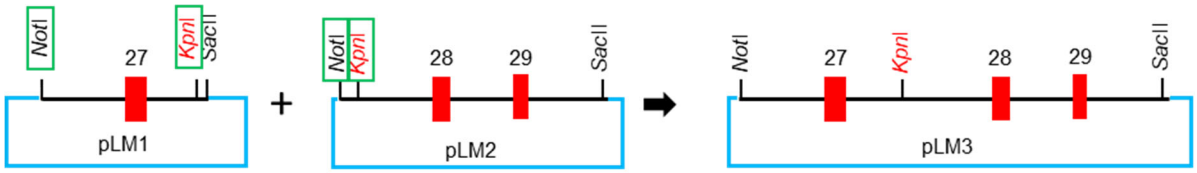

4) The middle homologous region was released from pLRRK1#3 (pLM3) using *Not*I and *Sac*II followed by Klenow to blunt the sticky ends, which was then subcloned into the *Sma*I site of pGKneoF2L2DTA (addgene: #13445) to generate pLRRK1#4 (pLM4).

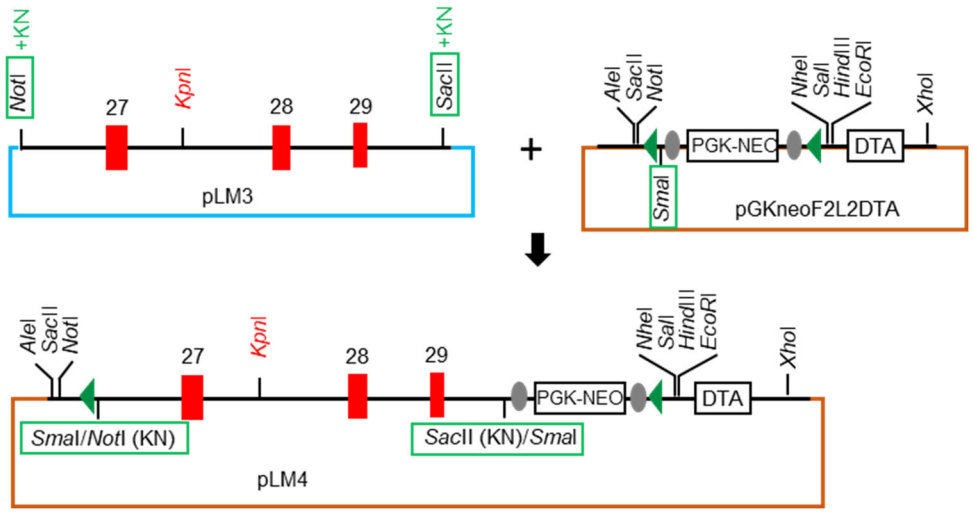

Green arrowhead: *loxP* site, gray circle: *FRT* site

5) The left arm was amplified from mouse BAC DNA (Clone: RP23-213J23) using primers P1 and P2. The resulting PCR product (2,016 bp) containing part of *LRRK1* intron 25, exon 26, and part of intron 26 was digested with *Sac*II and *Not*I, and was then subcloned into the *Sac*II and *Not*I sites of pGKneoF2L2DTA (addgene: #13445) to generate pLRRK1#5 (pLM5).

P1: 5'gacat*CCGCGG*CACCATGTGAGTGGCAGCTGTGGTGAGAAC (41 bp). *Sac*II (*CCGCGG*) is an exogenous site.

P2: 5'gacat*GCGGCCGCAAGCTT*TTTAATAGCCGTTCTTTCTTAGAGAAGGCAG (50 bp). *Not*I (*GCGGCCGC*) and *Hind*III (*AAGCTT*) are exogenous sites.

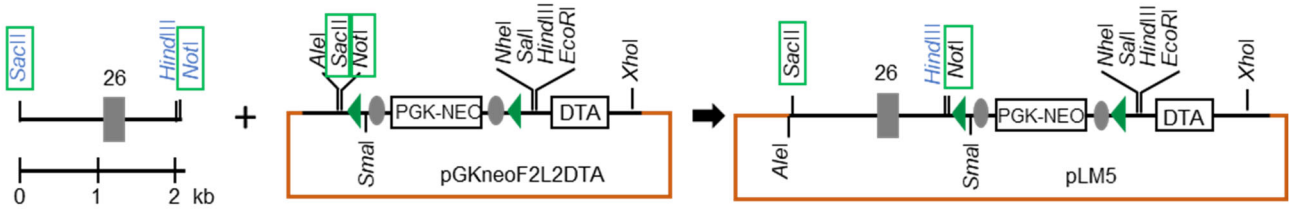

6) The right arm was amplified from mouse BAC DNA (Clone: RP23-213J23) using primers P7 and P8. The resulting PCR product (3,131 bp) containing part of *LRRK1* intron 29, exon 30, and part of intron 30 was digested with *Sal*I and *Hind*III, and was then subcloned into the *Sal*I and *Hind*III sites of pGKneoF2L2DTA (addgene: #13445) to generate pLRRK1#6 (pLM6).

P7: 5'gacat*GTCGAC*GGATCCGTAGGGAAGACCCACTAGGAGGAAGAAAG (46 bp). *Sal*I (*GTCGAC*) is an exogenous site.

P8: 5'gacat*AAGCTT*TGGTACCTTTCTAAAGGCAGCATTTTGCTTGC (43 bp). *Hind*III (*AAGCTT*) is an exogenous site.

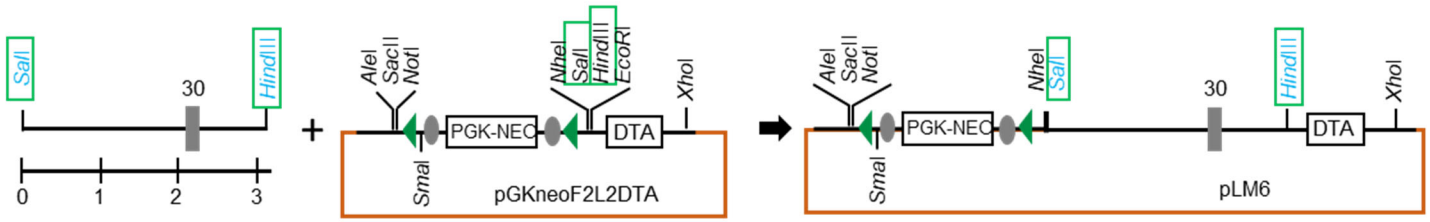

7) pLRRK1#5 (pLM5) was digested with *Sac*II and *Not*I, and was then subcloned into the *Sac*II and *Not*I sites of pLRRK1#6 (pLM6) to generate pLRRK1#7 (pLM7).

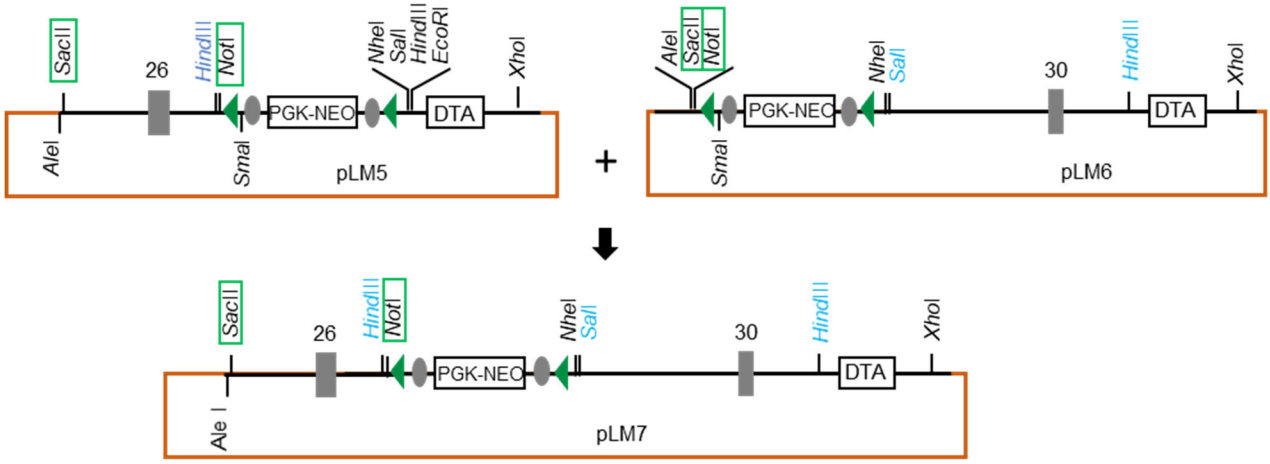

8) The middle homologous region was released from pLRRK1#4 by *Not*I and *Sal*I and was then subcloned into the *Not*I and *Sal*I sites of pLRRK1#7 (pLM7) to generate the final targeting vector pLRRK1#8 (pLM8), which was linearized with *Xho*I before electroporation into ES cells.

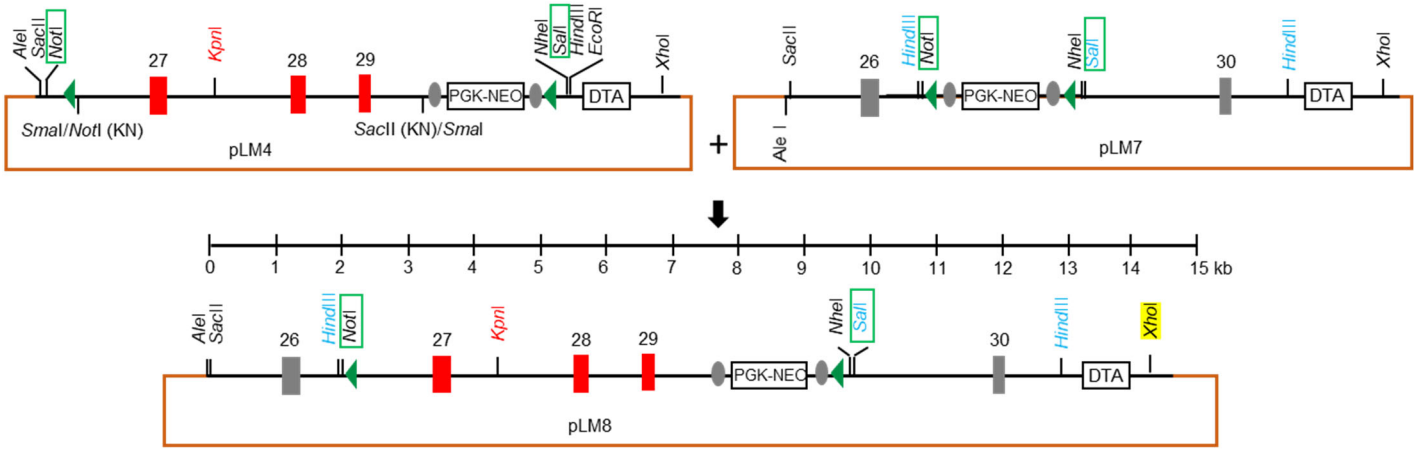

Restriction sites in black: from vectors

Restriction sites in red: *LRRK1* endogenous sites

Restriction sites in blue: introduced by the primers

Figure 1-figure supplement 2. Genomic DNA sequence of the floxed *LRRK1* allele

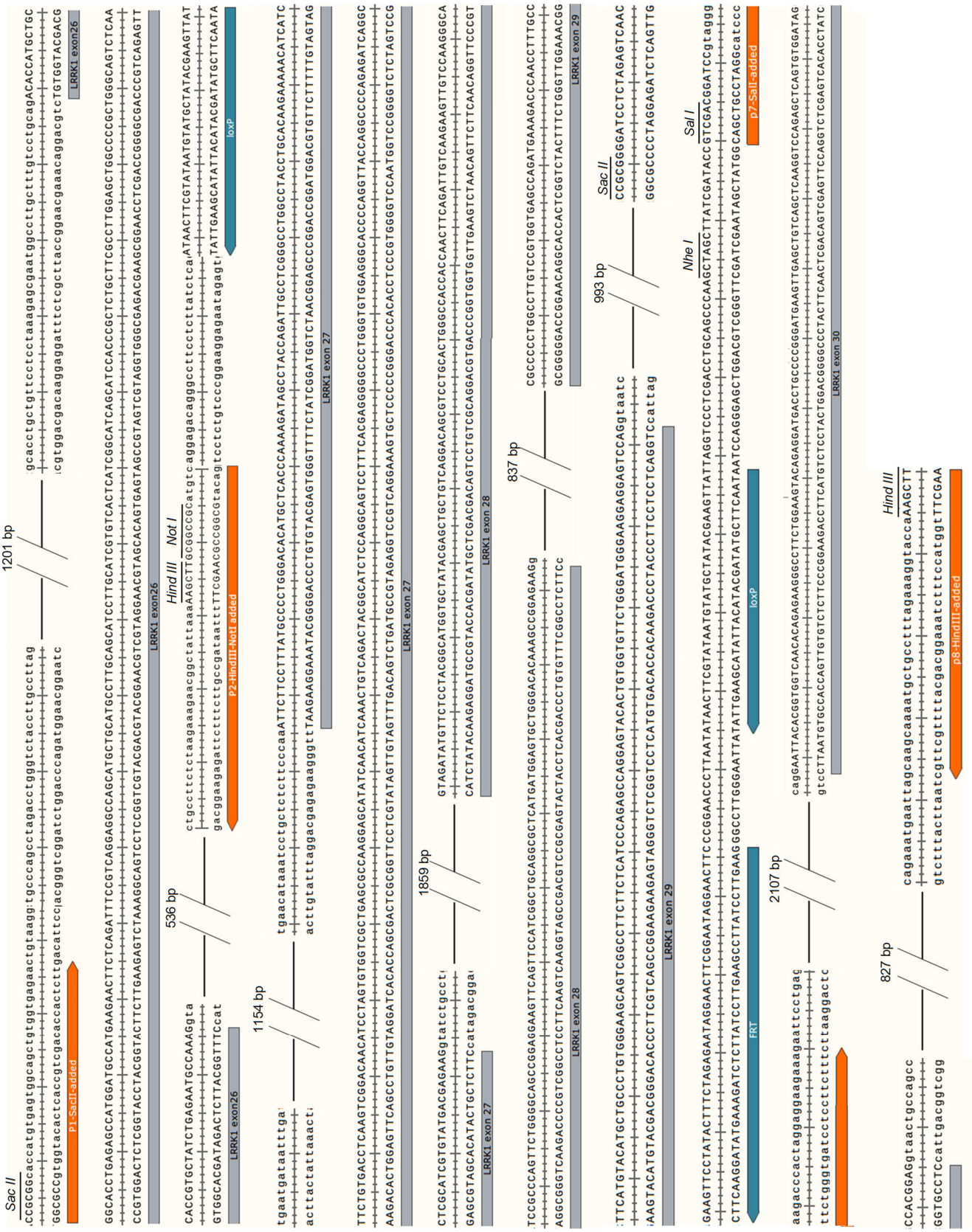

Figure 1-figure supplement 3. Southern strategy for the targeted and floxed *LRRK1* alleles

5' external probe: 377 bp (*LRRK1* intron 25)

P15: 5'CAGAATACCCCATGCTGGGGAATTGC (26 bp)

P16: 5'CCGTTTCTAGGATTCTAATTTTTC (24 bp)

Hind*III digestion** ***WT: 17.0 kb
Targeted: 4.8 kb
Floxed: 4.8 kb

3' external probe: 305 bp (*LRRK1* exon 32)

P17: 5'AACTCCTTCCTGGTGCTGGCAGGCCTGGCTG (31 bp)

P18: 5'ACAAGTGACGTGACCATGGACGGAGCTGCG (30 bp)

Hind*III digestion** ***WT: 17.0 kb
Targeted: 14.1 kb
Floxed: 12.2 kb

***Neo* probe (363 bp)**

P23: 5'ATTCGGCTATGACTGGGCAC (20 bp)

P24: 5'GACCACCAAGCGAAACATCG (21 bp)

Hind*III digestion** ***WT and Floxed: no band
Targeted: 14.1 kb

Figure 1-figure supplement 4. Generation of the *LRRK2* targeting vector

1) The left homologous region was amplified from mouse BAC DNA (Clone# RP23-526-A2, BACPAC Resources Center) using primers P9 and P10. The resulting PCR product (2,579 bp) was digested with *EcoR*I, which is an endogenous restriction site upstream of the *LRRK2* promoter, and was then subcloned into the *EcoR*I and *Sma*I sites of pBSK (+) to generate pLRRK2#1 (2,526 bp + 2,961 bp = 5,487 bp).

P9: 5' GAACACACAAGGCTATGGCTATTGTC (26 bp)

P10: 5' GTAGGACTATCATCCACCTGTAGGACTCC (29 bp)

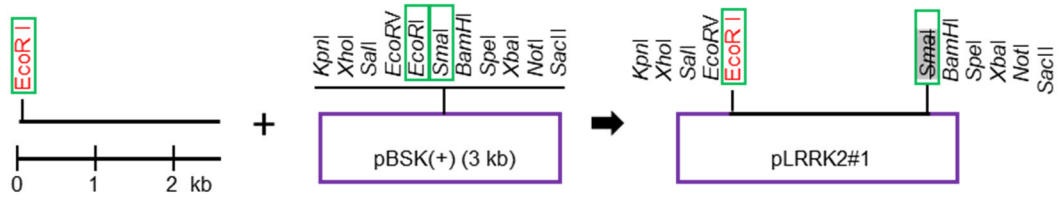

2) Oligoes (P39 and P40) were annealed together to generate a double stranded polylinker (*BamH*I-*loxP*-*Nhe*I-*Spe*I), which was then subcloned into the *BamH*I and *Spe*I sites of pLRRK2#1 to generate pLRRK2#2 (5,487 bp + 50 bp = 5,537 bp).

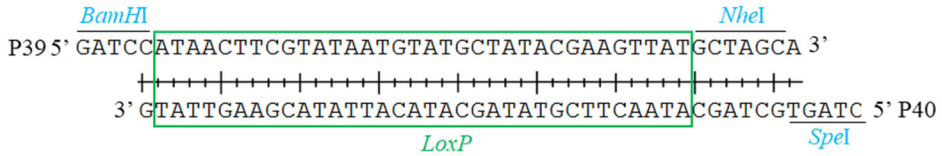

P39: 5' GATCCATAACTTCGTATAATGTATGCTATACGAAGTTATGCTAGCA (46 bp).
*BamH*I (G'GATCC), *loxP* top strand (ATAACTTCGTATAATGTATGCTATACGAAGTTAT), *Nhe*I (G'CTAGC).

P40: 5' CTAGTGCTAGCATAACTTCGTATAGCATACATTATACGAAGTTATG (46 bp).
*Spe*I (A'CTAGT), *Nhe*I (GCTAGC), *loxP* bottom strand (ATAACTTCGTATAGCATACATTATACGAAGTTAT).

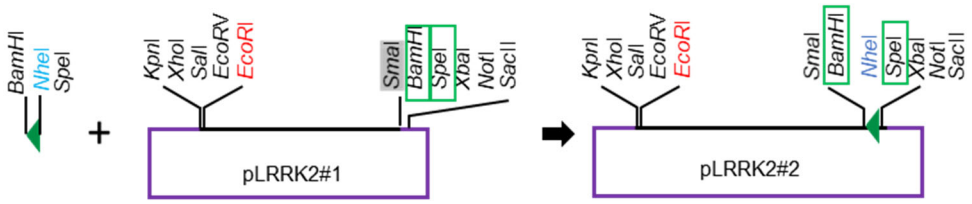

Green arrowhead: *loxP* site

3) The middle arm was amplified from mouse BAC DNA (Clone# RP23-526-A2) using primers P11 (upstream of the *LRRK2* promoter) and P12 (intron 2). The resulting PCR product (2,990 bp) was digested with *Xba*I and *Not*I and was then subcloned into the *Xba*I and *Not*I of pGEM-T Vector (Promega, Cat#: A1360) to generate pLRRK2#3 (2,990 bp + 3,000 bp = 5,990 bp). *Xba*I, *Not*I, and *Nhe*I sites are exogenous sequences introduced into PCR primers.

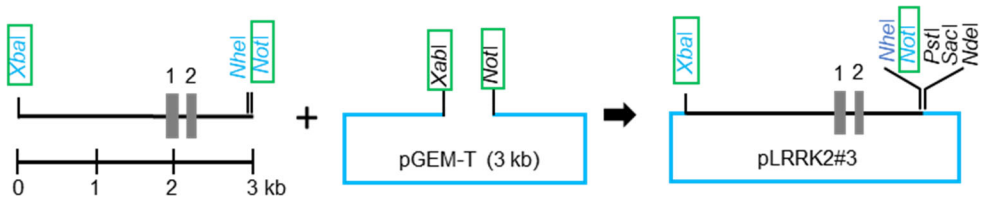

4) pLRRK2#3 was digested with *Xba*I and *Not*I, and the insert was then subcloned into the *Xba*I and *Not*I sites of pLRRK2#2, which contains the left homologous arm and the *loxP* sequence, to generate pLRRK2#4 (2,958 bp + 5,490 bp = 8,448 bp).

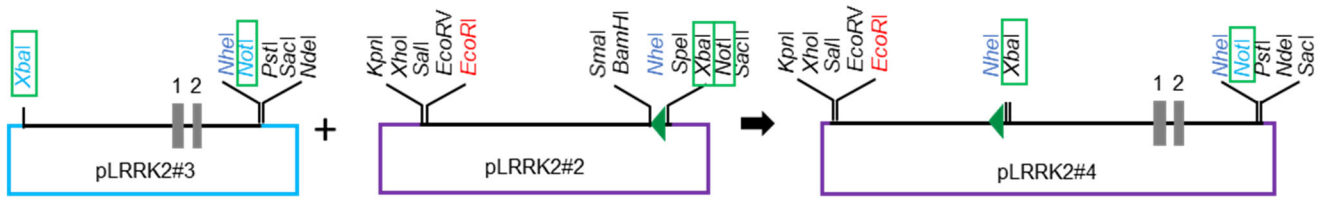

5) The right arm was amplified from mouse BAC DNA (Clone# RP23-526-A2) using primers P13 and P14. The resulting 3,503 bp PCR fragment containing *LRRK2* intron 1, exon 2, and intron 2, was subcloned into the *EcoR*V site of pBSK(+) to generate pLRRK2#5 (3,503 bp + 2,961 bp = 6,464 bp). **Check direction!!!**

PCR: P13=5'GCACTTGAGTCTTAATCTTGGGCAC 3' (25 bp)

P14=5'CATTCGAGCAGCTAAGCCTGTAATC 3' (25 bp)

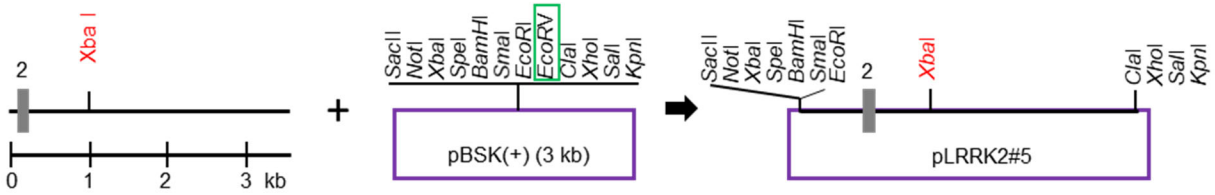

6) pLRRK2#5 was digested with *BamH*I and then treated with Klenow to blunt the overhang followed by *Cla*I digestion. The digested fragment was subcloned into the *EcoR*V and *Cla*I sites of the pSoriano vector (*PGKneolox2DTA*, addgene 13443) to generate pLRRK2#6 (3,547 bp + 6,307 bp = 9,854 bp).

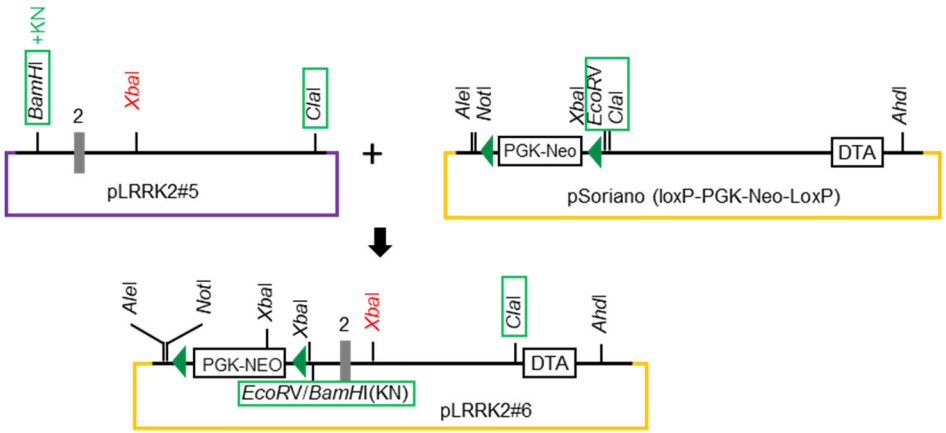

7) The LFNT-tk/pBS plasmid (a gift from S. Tonegawa) was digested with *Sac*II (followed by Klenow) and *Not*I (followed by *Ssp*I) to release the "*loxP-FRT-PGK-neo-loxP-FRT*" fragment (2,928 bp), which was then subcloned into the *Xba*I (followed by Klenow) and *Not*I sites of pLRRK2#6 to generate pLRRK2#7 (2,928 bp + 7,051 bp = 9,979 bp).

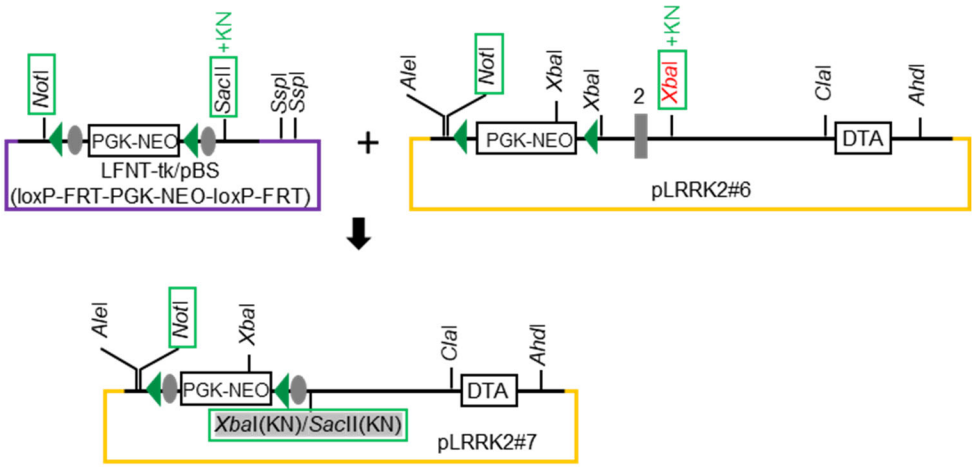

Green arrowhead: *loxP* site, gray circle: *FRT* site

8) pLRRK2#4 was digested with *EcoR*V and *Not*I to release the fragment containing the left arm-*loxP*-middle arm, which was then subcloned into the *Ale*I and *Not*I sites of pLRRK2#7 to obtain pLRRK2#8, the *LRRK2* targeting vector (15,485 bp). The linearized targeting vector (with *Ahd*I) was electroporated into ES cells.

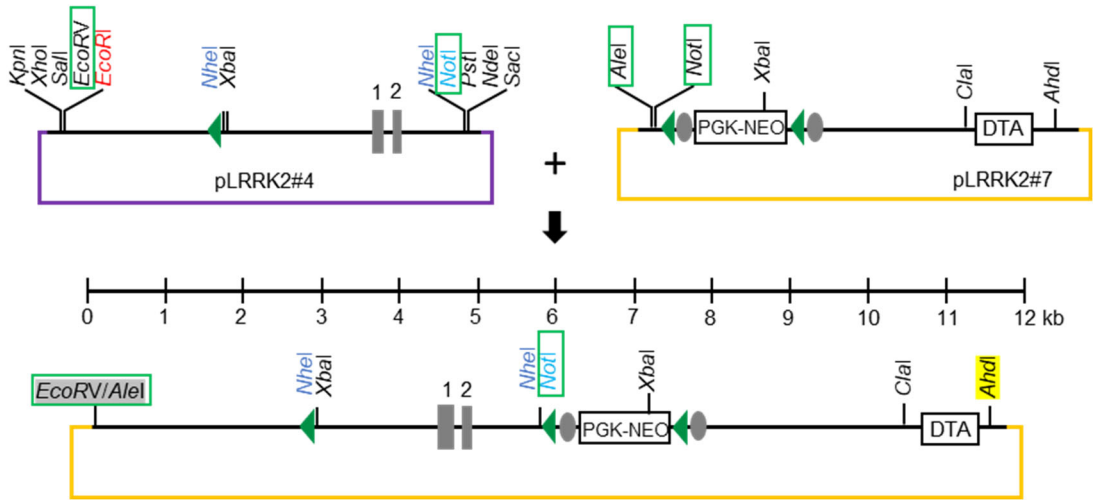

Restriction sites in black: from vectors

Restriction sites in red: *LRRK2* endogenous sites

Restriction sites in blue: introduced by the primers

Figure 1-figure supplement 5. Genomic DNA sequence of the floxed *LRRK2* allele

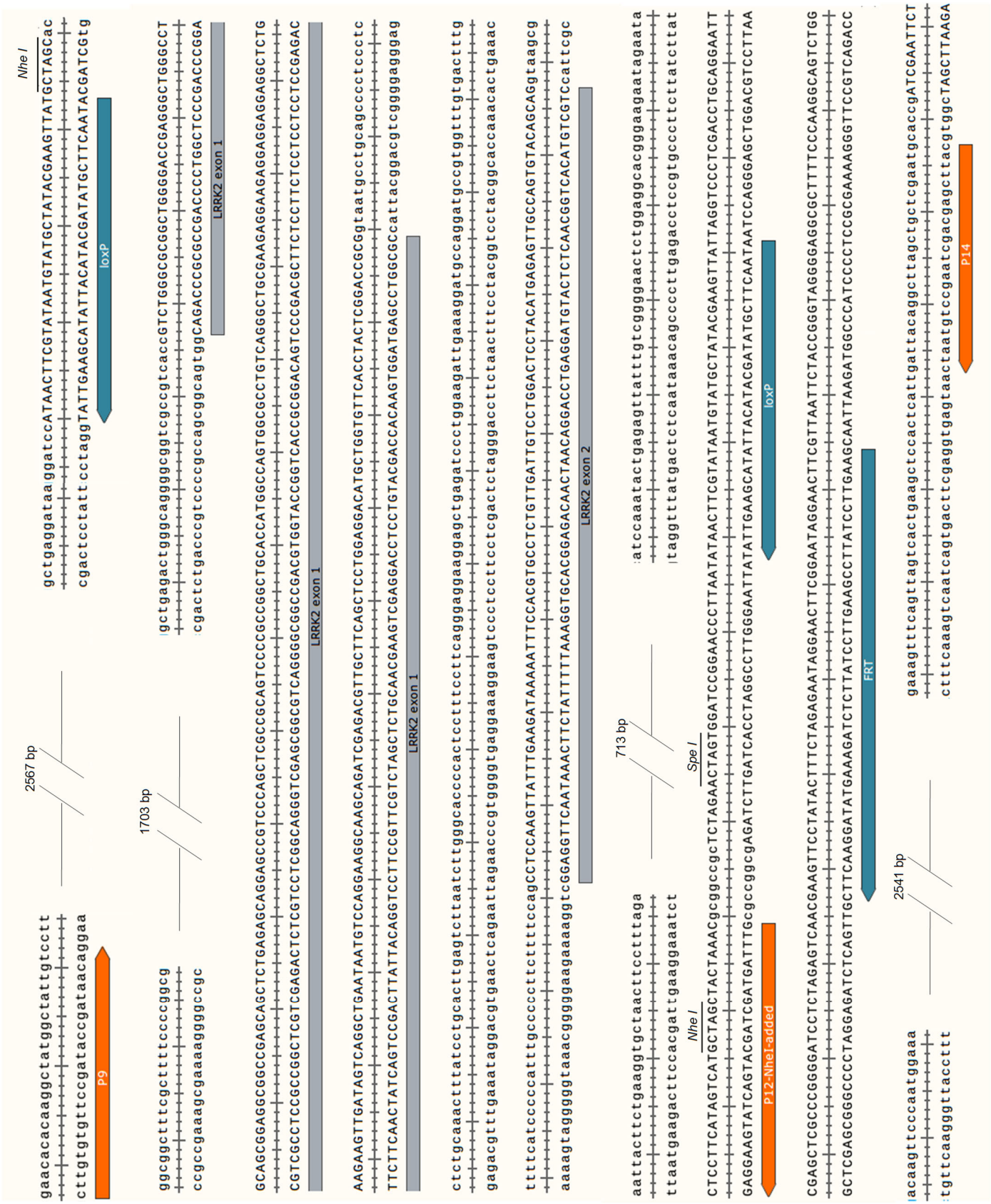

Figure 1-figure supplement 6. Southern analysis of the targeted and floxed *LRRK2* alleles

5' external probe (753 bp)

P19= 5'CATGGGAGAGAGGGTTTCTCACTTACT (27 bp)

P20= 5'CTTGGACAGCATTGTCAGCCTAGAC (25 bp)

Nhe*I digestion** ***WT: 11.5 kb
Targeted and floxed: 3.6 kb

3' external probe (622 bp)

P21=5' GCCAAGCAGTTATTGATGCTGTAGC (31 bp)

P22= 5' CGAGCTGTAAGATGAGCTGGGTACT (30 bp)

Sph*I digestion** ***WT: 12.3 kb
Targeted: 4.5 kb

Nhe*I digestion** ***WT: 11.5 kb
Floxed: 5.2 kb

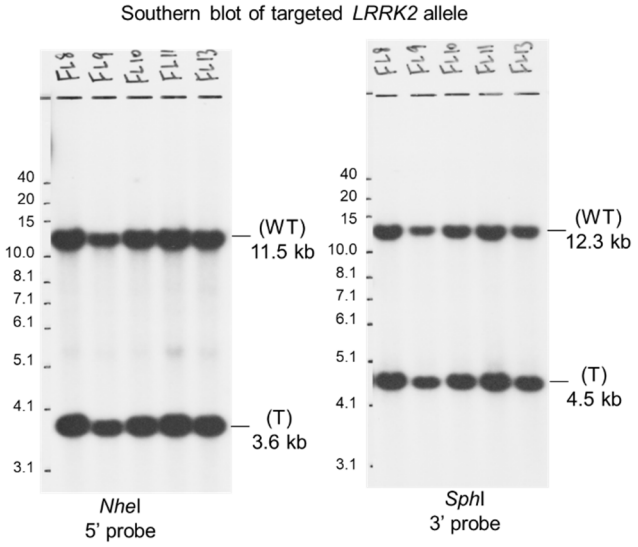

Figure 1-figure supplement 7. Northern strategy for *LRRK1* mRNA

***LRRK1* exons 2-3 probe (377+4=383 bp)**

P31: 5' CAGGATGAGCGTGTGTCTGCAG (CAG exon 1/rest exon2)

P32: 5′ CCTTCTCCTGTGAGGATTCGCTCT (C exon 3/rest exon 4)

WT and floxed alleles: ~7.4 kb

Deleted allele: ~6.8 kb*

* Deletion of *LRRK1* exons 27-29 (625 bp; exon 27: 278 bp, exon 28: 195 bp, exon 29 152 bp) results in a frameshift of downstream exons, likely resulting in degradation of the transcript.

***LRRK1* exons 27-29 probe (550 bp)**

P33: 5' CTGGCCTACCTGCACAAGAA (exon 27)

P34: 5' CCTTCCCATCCCAGAACACC (exon 29)

WT and floxed alleles: 7.4 kb

Deleted allele: no band

***GAPDH* probe (452 bp)**

P37: 5' ACCACAGTCCATGCCATCAC (exon 5)

P38: 5′ TCCACCACCCTGTTGCTGTA (exon 7)

Figure 1-figure supplement 8. Northern analysis of *LRRK1* mRNA in mice carrying *LRRK1* germline deleted alleles

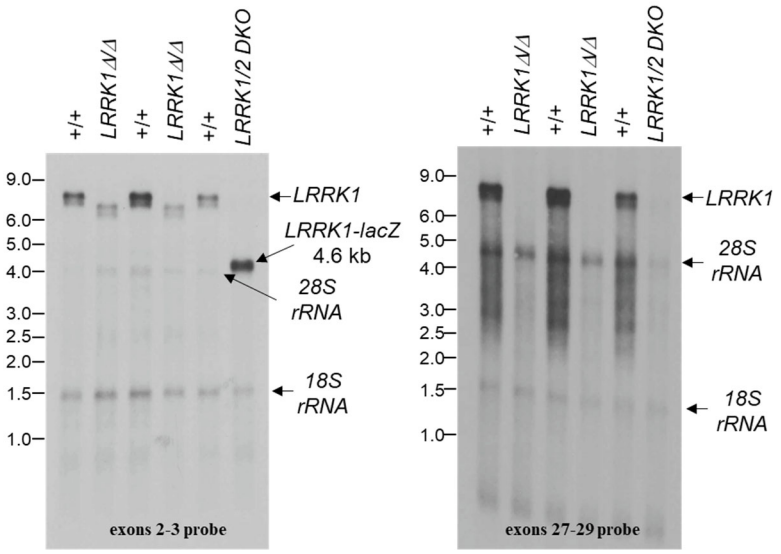

LRRK1 Northern blots (polyA+ RNA from the lung) using exons 2-3 or exons 27-29 probe: The exons 2-3 probe detected the full-length *LRRK1* transcripts (~7.4 kb) in wild-type (+/+) mice and reduced size transcripts in *LRRK1* Δ/Δ mice, likely due to the absence of exons 27-29 (625 bp), which was confirmed by sequencing of RT-PCR products (see Figure1-figure supplement 9). The truncated *LRRK1* mRNA lacking exons 27-29 is present in lower levels, likely due to mRNA degradation by nonsense-mediated decay, as the absence of exons 27-29 (625 bp) results in a frameshift of downstream codons.

The exons 2-3 probe also recognizes the fusion transcript *LRRK1-lacZ* (~4.6 kb) in *LRRK1/2* DKO mice, which contains *LRRK1* exons 1-3 and exon 2 of engrailed, *IRES* and *lacZ* cDNA (Figure 1, Figure S1 in Giaime et al., *Neuron*, 2017). The exons 27-29 probe also recognizes the full-length *LRRK1* transcripts (~7.4 kb) in wild-type (+/+) mice but no truncated *LRRK1* transcripts, due to the germline deletion of the genomic region from intron 26- intron 29, lacking exons 27-29. The exons 27-29 probe also did not detect the *LRRK1-lacZ* fusion transcript, which only contains exons 1-3, in *LRRK1/2* DKO mice. While polyA enrichment reduced levels of 18S and 28S rRNAs, they are still present in the lanes/samples.

Figure 1-figure supplement 9. RT-PCR analysis of the deleted *LRRK1* allele

RT-PCR analysis using a *LRRK1* exon 32-specific primer P47 (5'GGCTCAGGTCATGCTCAGTT) for RT and PCR primer sets in *LRRK1* exons 4-8, 11-17, 20-25, and 25-31 indicates normal splicing in homozygous floxed *LRRK1* (F/F) mice and properly deleted transcripts in *LRRK1* Δ/Δ mice. The identity of all PCR products was confirmed by sequencing.

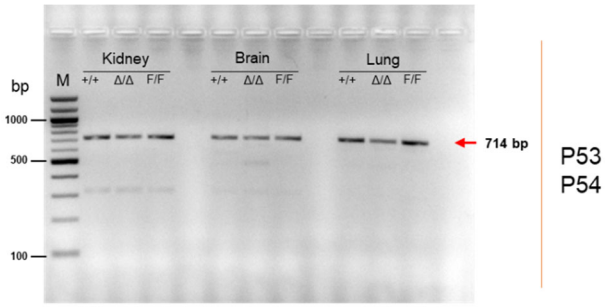

714 bp: Ex4(47)-Ex5(180)-Ex6(149)-Ex7(227)-Ex8(111)

P53: 5' TTTTGGACACGCCGAAGTAGT (**exon 4**)

P54: 5' AGCCGCTCCAGGTAGTTTTT (**exon 8**)

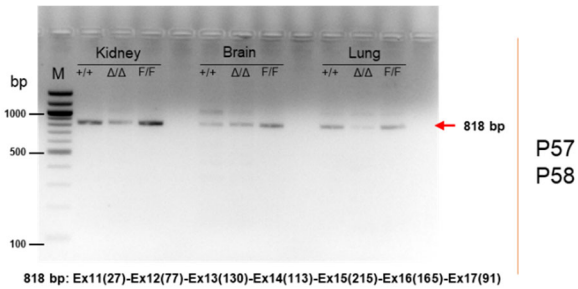

818 bp: Ex11(27)-Ex12(77)-Ex13(130)-Ex14(113)-Ex15(215)-Ex16(165)-Ex17(91)

P57: 5' GGACCTCTCCAGAAACCAGC (**exon 11**)

P58: 5' GCAGGGTTGCTATCCTCTCC (**exon 17**)

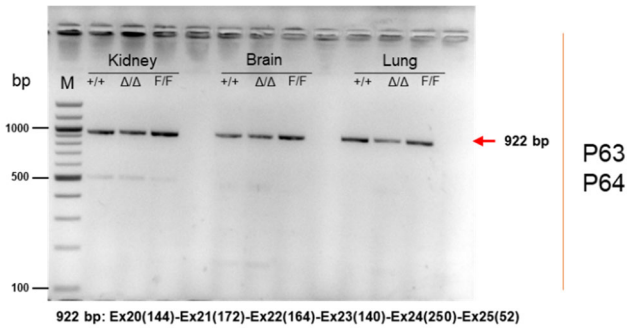

922 bp: Ex20(144)-Ex21(172)-Ex22(164)-Ex23(140)-Ex24(250)-Ex25(52)

P63: 5' GCGGTCAGTGGCAAAGAATG (**exon 20**)

P64: 5' AATGCTGTTCTCACCCTCCG (**exon 25**)

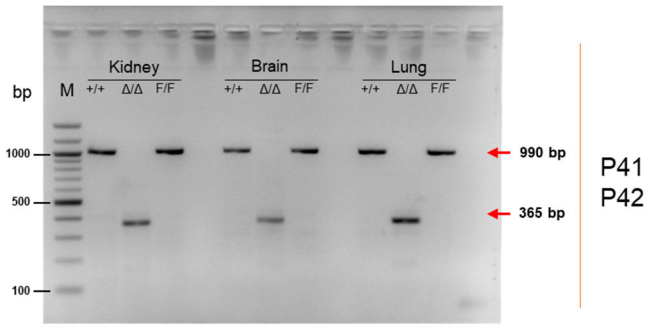

990 bp: wild-type exon 25 to 31
Ex25(23)-Ex26(198)-Ex27(278)-Ex28(195)-Ex29(152)-Ex30(118)-Ex31(26)
365 bp: deletion of exon 27 to 29
Ex25(23)-Ex26(198)-Ex30(118)-Ex31(26)

P41: 5' GAATTCTGCTAATGCCCCAGC (**exon 25**)

P42: 5' AGGCTGTAGATATAGATTTTCTGGT (**exon 31**)

The 990 bp product containing exons 25-31 represents the WT allele and confirms the floxed allele. The 365 bp product containing exons 25, 26, 30, and 31 confirms the deletion of exons 27-29.

Figure 1-figure supplement 10. Northern analysis of *LRRK2* mRNA in mice carrying floxed or germline deleted *LRRK2* alleles

***LRRK2* exons 1-5 probe (437 bp)**

P35= 5' AGGAAGGCAAGCAGATCGAG (exon 1, 20 bp)

P20= 5' GGCTGAATATCTGTGCATGGC (exon 5, 22 bp)

WT and floxed alleles: 8.3 kb
Deletion: no band

***GAPDH* probe (452 bp)**

P37= 5' ACCACAGTCCATGCCATCAC (exon 5, 20 bp)

P38= 5′ TCCACCACCCTGTTGCTGTA (exon 7, 20 bp)

LRRK2 Northern blot (total RNA from the brain) using exons 1-5 probe: The probe detected the full-length *LRRK2* transcript (~8.3 kb) in wild-type (+/+) and *fLRRK2/fLRRK2* mice, and no transcript in *LRRK2* Δ/Δ mice, derived from floxed *LRRK2* alleles, and previously generated *LRRK1/2* DKO mice (Giaime et al., *Neuron*, 2017).

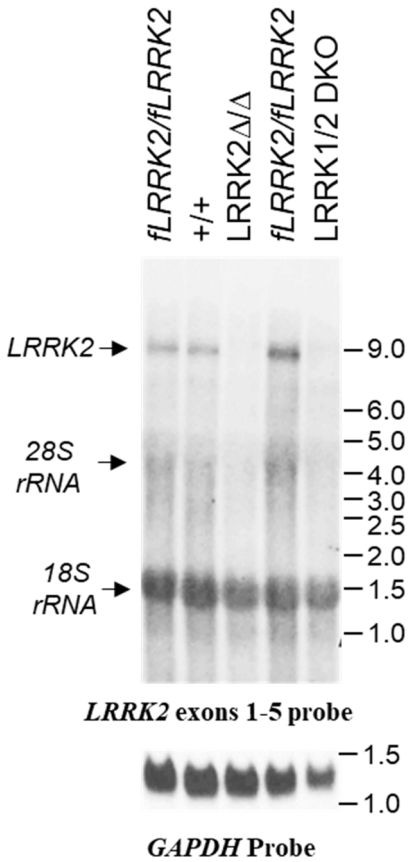

Figure 1-figure supplement 11. RT-PCR analysis of the deleted *LRRK2* allele
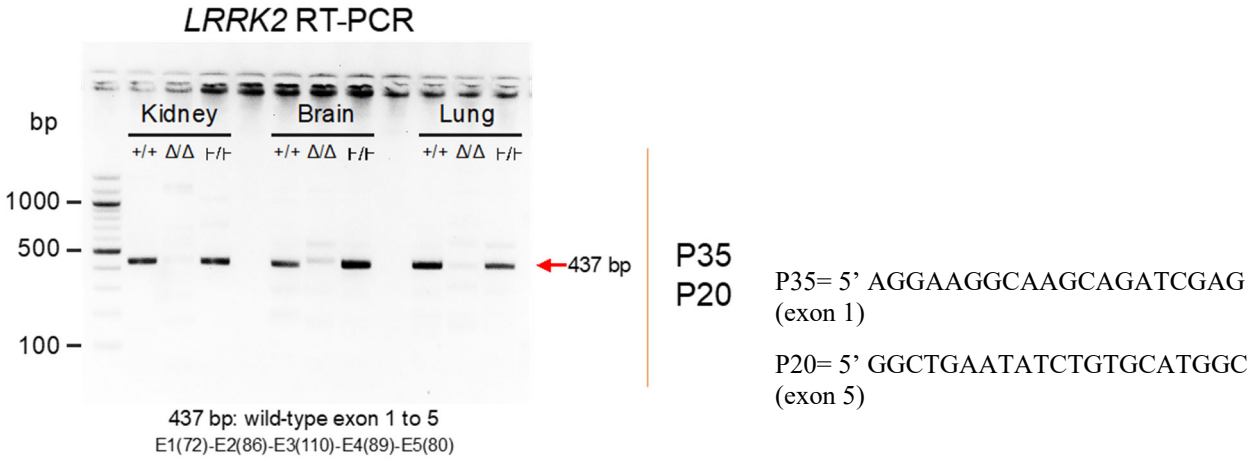
RT-PCR analysis using an *LRRK2* exon 51-specific primer P93 (5'TCGTGTGGAAGATTGAGGTCC) for RT, and primers in *LRRK2* exons 1 and 5, P35 and P20, for PCR, which shows normal splicing in *fLRRK2/fLRRK2* brains and the absence of PCR products in *LRRK2* Δ/Δ brains. The identity of the PCR product in +/+ and *fLRRK2/fLRRK2* brains was confirmed by sequencing: The 437 bp product contains *LRRK2* exons 1-5.